JOC The Journal of Organic Chemistry

pubs.acs.org/joc Article

Development and Application of a Peroxyl Radical Clock Approach for Measuring Both Hydrogen-Atom Transfer and Peroxyl Radical Addition Rate Constants

Quynh Do, David D. Lee, Andrew N. Dinh, Ryan P. Seguin, Rutan Zhang, and Libin Xu*

Cite This: J. Org. Chem. 2021, 86, 153−168 Read Online

ACCESS | Metrics & More | Article Recommendations | Supporting Information

ABSTRACT: The rate-determining step in free radical lipid peroxidation is the propagation of the peroxyl radical, where generally two types of reactions occur: (a) hydrogen-atom transfer (HAT) from a donor to the peroxyl radical; (b) peroxyl radical addition (PRA) to a "C═C" double bond. Peroxyl radical clocks have been used to determine the rate constants of HAT reactions (k_H), but no radical clock is available to measure the rate constants of PRA reactions (k_{add}). In this work, we modified the analytical approach on the linoleate-based peroxyl radical clock to enable the simultaneous measurement of both k_H and k_{add}. Compared to the original approach, this new approach involves the use of a strong reducing agent, $LiAlH_4$, to completely reduce both HAT and PRA-derived products and the relative quantitation of total linoleate oxidation products with or without reduction. The new approach was then applied to measuring the k_H and k_{add} values for several series of organic substrates, including para- and meta-substituted styrenes, substituted conjugated dienes, and cyclic alkenes. Furthermore, the k_H and k_{add} values for a variety of biologically important lipids were determined for the first time, including conjugated fatty acids, sterols, coenzyme Q10, and lipophilic vitamins, such as vitamins D_3 and A.

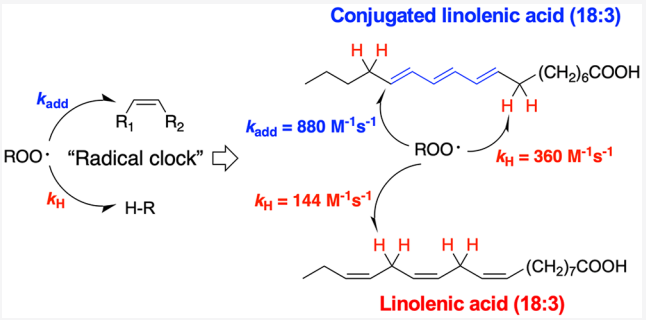

INTRODUCTION

Despite the crucial role of molecular oxygen in cell metabolism and energy production, imbalance between pro-oxidant and antioxidant cellular processes can lead to an increased level of reactive oxygen species, a state generally called "oxidative stress". Oxidative stress can result in DNA damage and alter cell proliferation, differentiation, or metabolism.[1] Lipids are among the primary targets of attack by reactive oxygen species, leading to subsequent free radical chain reactions with molecular oxygen, termed lipid peroxidation. Since lipids are essential components of the cell membrane, lipid peroxidation is associated with multiple human conditions and diseases,[2−4] including atherosclerosis,[5] diabetes,[6] cancer,[7,8] neurodegenerative disorders,[9−11] and certain cholesterol biosynthesis disorders.[12] More recently, lipid peroxidation was discovered to be associated with ferroptosis, a regulated form of cell death that is morphologically, biochemically, and genetically distinct from other types of cell death such as apoptosis, necrosis, and autophagy.[13,14] More importantly, nonenzymatic lipid peroxidation, or autoxidation, was found to be the key effector in the induction of ferroptosis.[15−17]

The lipid autoxidation mechanism, kinetics, and product distribution have been studied intensively for decades.[2,4,18,19] The autoxidation process occurs via a three-step mechanism including the following: initiation, propagation, and termination (Figure 1).[2,4] The rate-limiting step in this mechanism is the propagation step in which the lipid peroxyl radical can undergo two types of reactions: hydrogen (H)-atom transfer (HAT) and peroxyl radical addition (PRA). In the HAT reaction, the peroxyl radical abstracts a H atom from another lipid or oxidizable substrate, generating a lipid hydroperoxide, while in the PRA reaction, the peroxyl radical adds to a "C═C" double bond. This PRA product can then either undergo intramolecular homolytic substitution (S_Hi) to form an epoxide or react with another molecular oxygen to form a new peroxyl radical. Both the HAT and PRA reactions generate new radicals that can continue the free radical chain oxidation by reacting with another lipid molecule or oxidizable substrate.

The direct measurement of HAT rate constants, k_H, for a variety of organic substrates requires the knowledge of the rates of polymerization (R_p), initiation (R_i), and termination (R_t); however, R_t can only be determined using the rotating-sector method.[20−22] On the other hand, a radical clock, which

Received: August 8, 2020
Published: December 3, 2020

https://dx.doi.org/10.1021/acs.joc.0c01920
J. Org. Chem. 2021, 86, 153−168

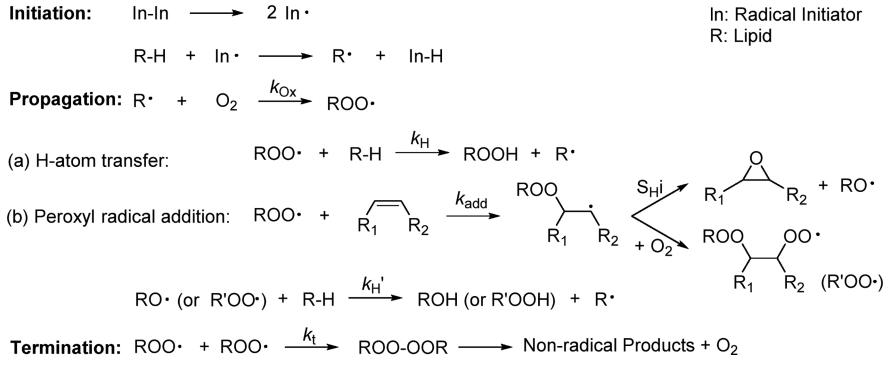

Figure 1. Sequence of the free radical chain oxidation of lipids.

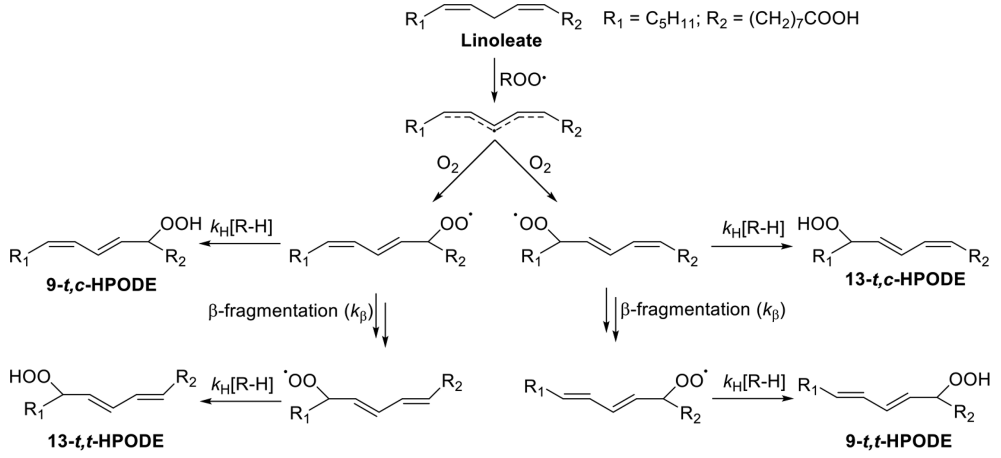

Figure 2. Original linoleate peroxyl radical clock.[23]

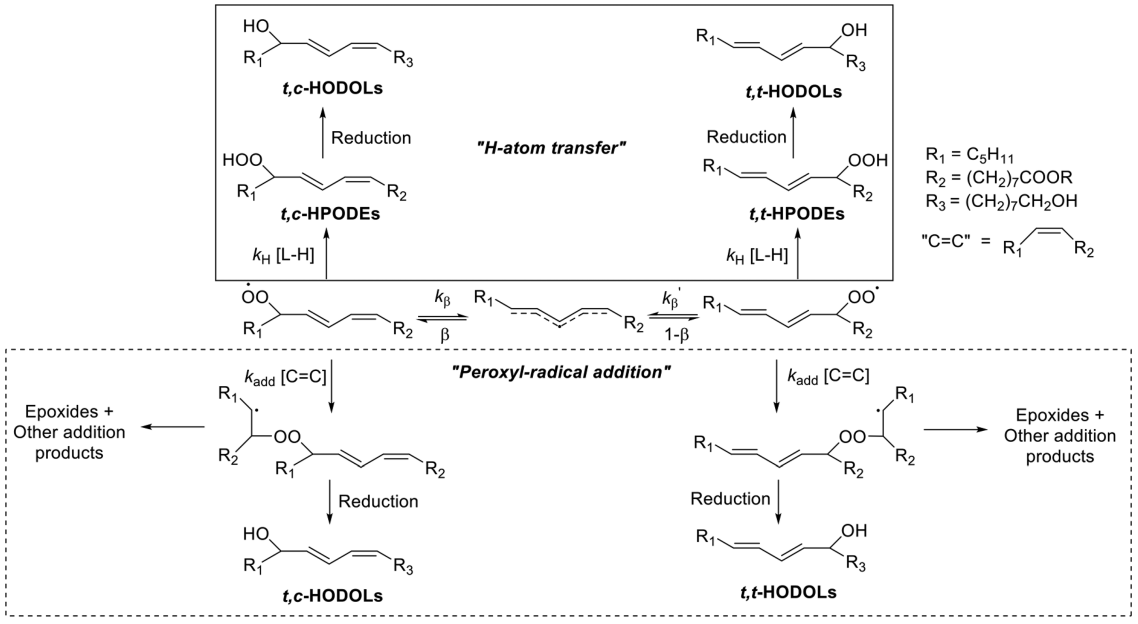

Figure 3. Linoleate peroxyl radical clock in the presence of both HAT and PRA reactions.

utilizes a known rate constant of a unimolecular reaction to measure an unknown rate constant of a competing bimolecular reaction, is a more convenient method to indirectly measure k_H.[23−26] Specifically, a linoleate-based peroxyl radical clock, which utilizes the competition between the β-fragmentation reactions with known rate constants and the bimolecular HAT reaction, was developed to measure k_H for a variety of lipids, including polyunsaturated fatty acids (PUFAs) and sterols (Figure 2).[23−26] Particularly, the reaction between linoleate and molecular oxygen can generate peroxyl radicals at either the 9- or 13-position of the carbon chain. These 9- or 13-peroxyl radicals can then undergo HAT to yield either 9-*trans*,

https://dx.doi.org/10.1021/acs.joc.0c01920
J. Org. Chem. 2021, 86, 153−168

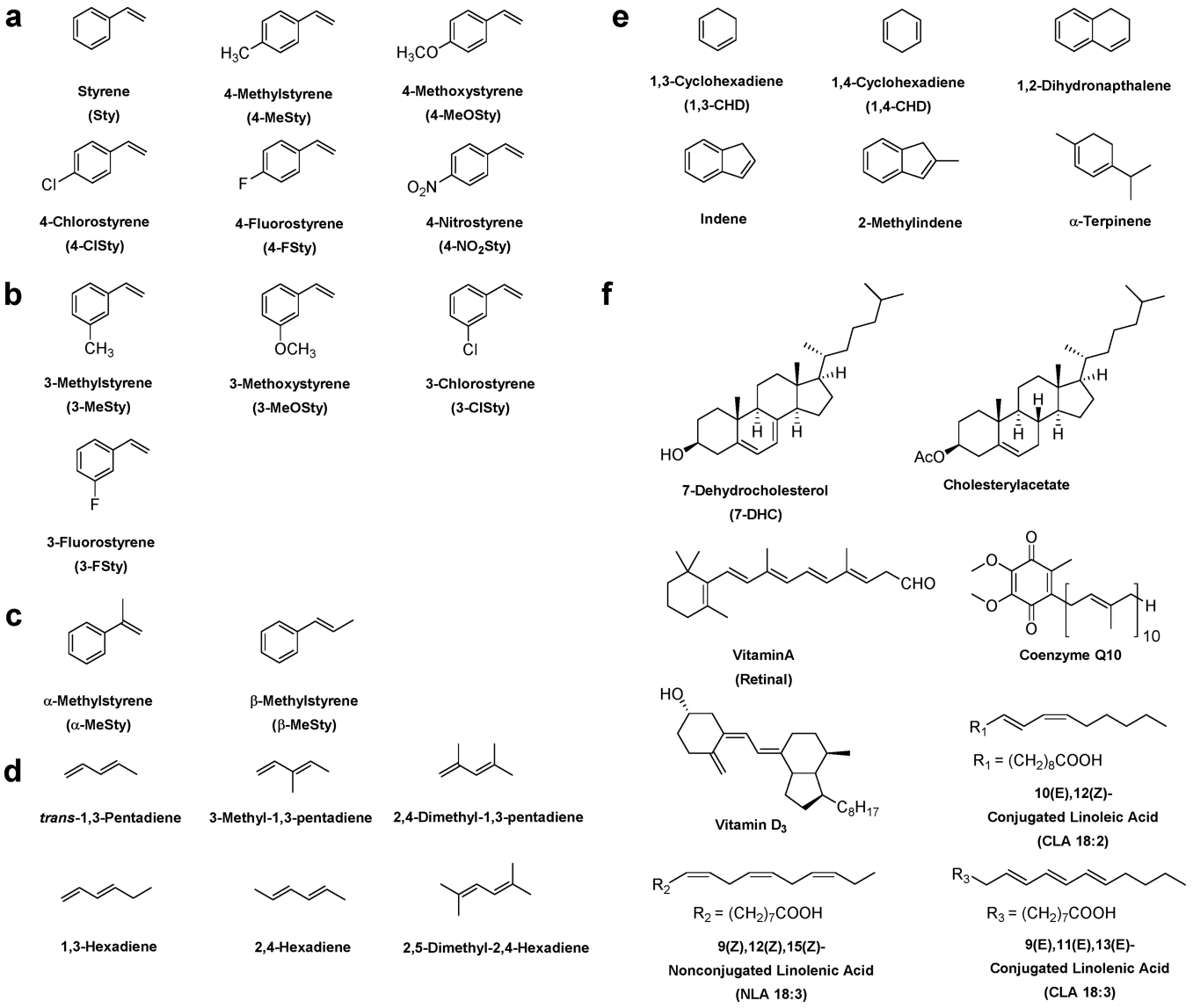

Figure 4. Series of substrates that are examined in this study: (a) styrene and its para-substituted derivatives, (b) meta-substituted styrene derivatives, (c) styrenes with methyl substituent at the α- and β-position, (d) conjugated dienes with different methyl substituents, (e) cyclic hydrocarbons, and (f) biologically important lipids.

cis (*t,c*)- or 13-*t, c*-hydroperoxide products, which are termed HPODEs, or they can also undergo the competing β-fragmentation reaction, leading to 13-*trans, trans* (*t,t*)- and 9-*t,t*-HPODEs. Therefore, linoleate peroxyl radicals, with known rate constants for β-fragmentation, can be used to "clock" the unknown rate constants of HAT reactions via eq 1:

$$\frac{[t,\,c\text{-HPODEs}]}{[t,\,t\text{-HPODEs}]} = \frac{[9\text{-}t,\,c\text{-HPODEs} + 13\text{-}t,\,c\text{-HPODEs}]}{[9\text{-}t,\,t\text{-HPODEs} + 13\text{-}t,\,t\text{-HPODEs}]} = \frac{k_H[\text{Substrate}]}{214} + 0.16 \quad (1)$$

Here, 214 and 0.16 are β-fragmentation-dependent constants.[23] Based on the measurements using the peroxyl radical clock method, cholesterol was found to be a moderately oxidizable lipid with a k_H of 11 M^{-1} s^{-1} at 37 °C, but 7-dehydrocholesterol (7-DHC), a biosynthetic precursor of cholesterol and vitamin D_3,[27,28] was found to be the most reactive lipid molecule so far, with a k_H of 2260 M^{-1} s^{-1}.[24]

While the HAT reaction mechanism and rate constants have been studied extensively via the radical clock method, there has not been any method established to measure the rate constants for the PRA reaction, k_{add}. Epoxides, one of the addition products, were identified among the oxidation products from sterols, such as cholesterol and 7-DHC.[12,29,30] In addition, intramolecular PRA reactions were discovered to occur in cardiolipins with multiple linoleate chains, once one chain is oxidized to linoleate peroxyl radical.[31] This is evidence that PRA also contributes significantly to the propagation step, and thus, its rate constants should also be considered in the study of lipid peroxidation kinetics. This is a major gap in the field that this study aims to fill. The sum of k_H and k_{add}, also defined as the total propagation rate constant (k_p) of the lipid peroxidation of a substrate, can also be measured with the inhibited autoxidation method using a set of calibrated reference inhibitors.[32] However, this method cannot differentiate between the two rate constants either. To fully understand the complex nature of the lipid peroxidation mechanism, kinetics, and products, we modified the current

https://dx.doi.org/10.1021/acs.joc.0c01920
J. Org. Chem. 2021, 86, 153−168

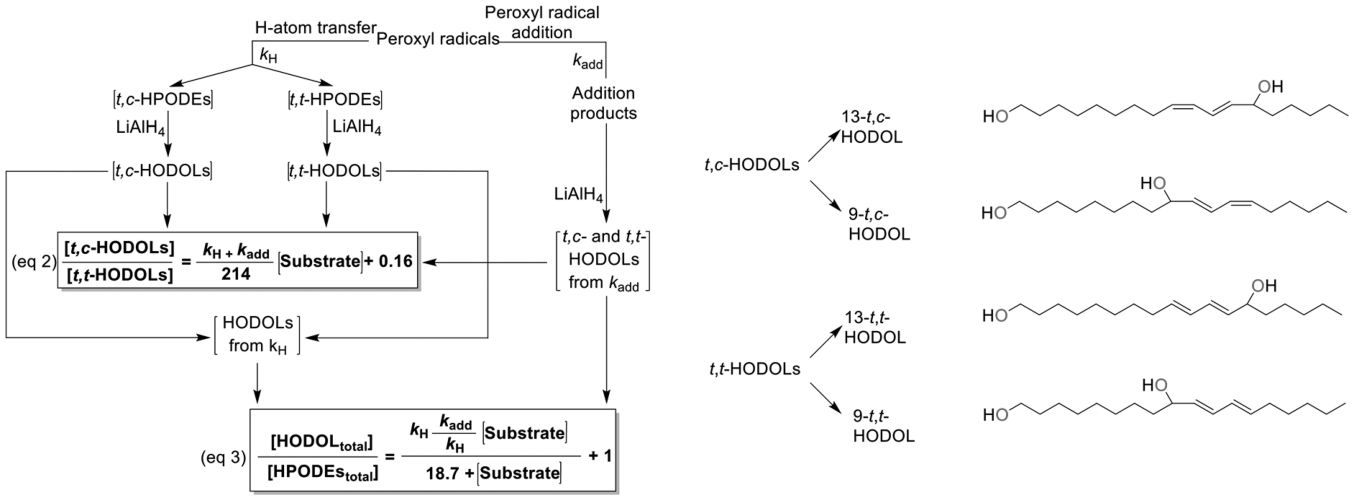

Figure 5. Proposed new radical clock approach and the structures of 13-*t,c*-, 9-*t,c*-, 13-*t,t*-, and 9-*t,t*-HODOL. (HPODE: hydroperoxyoctadecadienoic acid, i.e., nonreduced products from HAT reaction; HODOL: hydroxyoctadecadienol, i.e., reduced products from both HAT and PRA reactions; *t,c*: *trans, cis*; *t,t*: *trans, trans*; k_H: HAT rate constant; k_{add}: PRA rate constant.)

linoleate peroxyl radical clock to account for the contribution of the PRA reaction (Figure 3).

We report here the development of a new analytical approach based on the original linoleate-based peroxyl radical clock, which enables the simultaneous measurement of the rate constants of both HAT and PRA reactions. We first explain the design of the new peroxyl radical clock approach. We then apply this new approach to elucidate the values of k_H and k_{add} for a variety of substrates, including para- and meta-substituted styrenes, double bond-substituted styrenes, conjugated dienes with methyl substituent at different positions, cyclic compounds, and biologically important lipids (Figure 4). Based on these results, we will discuss the factors that affect the contribution of each reaction to the overall propagation step. In the end, we will discuss the limitations and the biological implications of the new approach.

RESULTS

Design of the New Peroxyl Radical Clock. Our new approach was developed based on the autoxidation of methyl linoleate (MeLn) as its mechanism is well studied. In addition, our preliminary studies had shown that the high-performance liquid chromatography (HPLC) chromatograms of MeLn-based oxidation products had better separation compared to that of linoleic acid, which enables better product analysis. To elucidate the values of k_H and k_{add}, it is crucial to capture all the linoleate-derived peroxide products by fully reducing the hydrogen peroxyl group in HPODEs from the HAT reaction and the alkyl peroxyl group in addition products from the PRA reaction. We used the co-oxidation reaction of MeLn and styrene in benzene to examine different reducing agents and conditions because styrene can only undergo PRA reactions (see the Experimental Section). After the peroxidation reaction, the reaction mixture was split into two halves. While the first half was analyzed directly, the second half was reduced prior to analysis. This ratio between the total reduced oxidation products and the total nonreduced oxidation products is expected to be equal to or larger than one if all the oxidation products are fully reduced. Even though triphenylphosphine was commonly used in the classic radical clock approach as a reducing agent,[23,24] we found that it was not strong enough to reduce all the linoleate-derived products, particularly those from the PRA reactions, which are dialkylperoxides and sometimes in the form of peroxide polymers.[2] Attempts using sodium borohydride under various conditions were also unsuccessful, leading to the ratios between the concentration of reduced and nonreduced oxidation products that are less than one. We found that the complete reduction of all oxidation products could only be achieved using the strong reducing agent lithium aluminum hydride ($LiAlH_4$). It should be noted here that $LiAlH_4$ reduces both the peroxyl bonds and the ester moiety in MeLn to alcohols. Importantly, these diols are a completely new set of products from the oxidation of linoleate that have never been characterized before as readouts for radical clocks. We termed these linoleate-derived alcohols, or hydroxyoctadecadienols, HODOLs (structures shown in Figure 5).

Our new peroxyl radical clock approach can be summarized into two main steps: to measure the sum of k_H and k_{add} and to determine the ratio of k_{add}/k_H (Figure 5). The sum of k_H and k_{add}, which is equal to k_p, can be elucidated via plotting the ratio [*t,c*-HODOLs]/[*t,t*-HODOLs] at different substrate concentrations. Specifically, when an oxidizable substrate can undergo both HAT and PRA reactions, the ratio [*t,c*-HODOLs]/[*t,t*-HODOLs] will be mediated by the competition from the HAT, β-fragmentation, and PRA reactions. Therefore, k_p can now be calculated from eq 2:

$$\frac{[t,\,c\text{-HODOLs}]}{[t,\,t\text{-HODOLs}]} = \frac{k_p[\text{Substrate}]}{214} + 0.16 \qquad (2)$$

On the other hand, the ratio k_{add}/k_H could be elucidated by plotting the ratio between the concentration of the total HODOLs, which are reduced oxidation products derived from both the HAT and PRA reactions, termed $HODOL_{total}$, and of the total HPODEs, which are nonreduced oxidation products derived from only the HAT reaction, termed $HPODE_{total}$, at different substrate concentrations. Thus, eq 3 describes the ratio $[HODOL_{total}]/[HPODE_{total}]$ as a function of substrate concentration.

https://dx.doi.org/10.1021/acs.joc.0c01920
J. Org. Chem. 2021, 86, 153−168

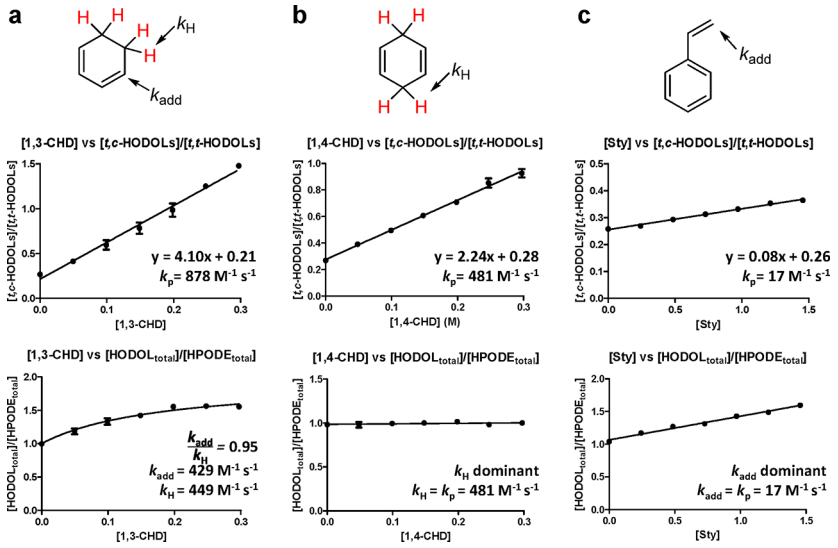

Figure 6. Determination of k_H and k_{add} for a substrate that can undergo (a) both reactions, (b) HAT reaction only, and (c) PRA reaction only. Here, the k_p value is calculated using the slope of the [Substrate] vs [*t,c*-HODOLs]/[*t,t*-HODOLs]. The ratio k_{add}/k_H is generated from the fitting of the [Substrate] vs [$HODOL_{total}$]/[$HPODE_{total}$] plot using Prism. The measurement for each substrate was performed in triplicate.

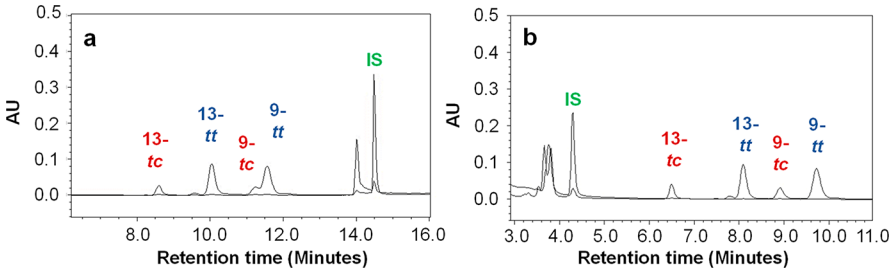

Figure 7. HPLC chromatogram at 234 nm for the (a) HPODE and (b) HODOL products eluting with solvent hexane:isopropyl alcohol = 99.5:0.5 and 95.5:4.5, respectively. The internal standard peak was monitored at 254 nm.

$$\frac{[HODOL_{total}]}{[HPODE_{total}]} = \frac{k_{MeLn}[MeLn] + k_H[Substrate] + k_{add}[Substrate]}{k_{MeLn}[MeLn] + k_H[Substrate]} = \frac{k_{add}[Substrate]}{k_{MeLn}[MeLn] + k_H[Substrate]} + 1 = \frac{k_H\frac{k_{add}}{k_H}[Substrate]}{k_{MeLn}[MeLn] + k_H[Substrate]} + 1 = \frac{k_H\frac{k_{add}}{k_H}[Substrate]}{18.7 + k_H[Substrate]} + 1 \quad (3)$$

Here, k_{MeLn} represents the total propagation rate constant of MeLn, which is 62 M^{-1} s^{-1} as measured by the rotating-sector method.[22] In addition, [MeLn], which is fixed at 0.3 M, is the concentration of MeLn used to set up the radical clock experiment. Therefore, the term k_{MeLn}[MeLn] is a constant that is equal to 18.7 s^{-1}. By fitting the [Substrate] vs [$HODOL_{total}$]/[$HPODE_{total}$] curve to eq 3 using Prism software, we could obtain the value of k_{add}/k_H. Now, the individual value for each rate constant could be solved from the sum and the ratio of k_H and k_{add}. An example on the determination of k_p, k_{add}, and k_H values from the [Substrate] vs [*t,c*-HODOLs]/[*t,t*-HODOLs] and [Substrate] vs [$HODOL_{total}$]/[$HPODE_{total}$] plots for 1,3-cyclohexadiene (1,3-CHD), a substrate that can undergoes both reactions, is shown in Figure 6a. When a substrate can only undergo the HAT reaction, such as 1,4-CHD, eq 3 would be rewritten as eq 4 and the linear fit of the [Substrate] vs [$HODOL_{total}$]/[$HPODE_{total}$] data would give a slope close to 0 (Figure 6b). In this case, the value of k_H would be reported as the value of k_p. In contrast, when PRA is predominant compared to HAT, such as in the oxidation of styrene (Sty), eq 3 would become eq 5, and the linear fit of [Substrate] vs [$HODOL_{total}$]/[$HPODE_{total}$] data would give a nonzero slope (Figure 6c). Here, the value of k_{add} would be equal to the value of k_p.

$$k_H\text{dominant:} \quad \frac{[HODOL_{total}]}{[HPODE_{total}]} = 1 \quad (4)$$

$$k_{add}\text{dominant:} \quad \frac{[HODOL_{total}]}{[HPODE_{total}]} = \frac{k_{add}[Substrate]}{18.7} + 1 \quad (5)$$

For this new peroxyl radical clock approach, normal phase HPLC/UV was utilized to quantify the relative amounts of HPODE and HODOL products, respectively, to an internal standard, 9-anthracenemethanol (Figure 7) (see the Experimental Section).

Application of the New Peroxyl Radical Clock Approach to Examining the Reactivities of Substrates That Can Only Undergo the PRA Mechanism. We first

https://dx.doi.org/10.1021/acs.joc.0c01920
J. Org. Chem. 2021, 86, 153−168

applied the new approach to measure the rate constants of para- and meta-substituted styrenes (Figure 4a and b). Since styrene and its para- and meta-substituted derivatives can only undergo PRA in reactions with MeLn, this series is useful not only in assessing the application of the new approach but also in determining the substituent effects on the reactivity of the PRA mechanism. The [Substrate] vs [$HODOL_{total}$]/[$HPODE_{total}$] curve for styrene and its derivatives confirmed that they are indeed k_{add} dominant (Figure S1 in the Supporting Information). The value of k_{add}, which is equal to k_p, for each compound was determined and is reported in Table 1. We found that the experimental k_{add} value of styrene is on the same order of magnitude as the value measured previously using the rotating-sector method at 30 °C.[33]

Table 1. PRA Rate Constants (k_{add}) and Activation Energies (E_a) of Para- and Meta-Substituted Styrene Derivatives at 37 °C

substrate	k_{add} (M^{-1} s^{-1})	E_a (kcal/mol)	lit. k_{add} (M^{-1} s^{-1})
Sty	17 ± 1	19.5	41[a]
4-MeSty	24 ± 1	19.2	na
4-MeOSty	56 ± 3	18.8	na
4-ClSty	17 ± 2	19.4	na
4-FSty	17 ± 2	19.5	na
4-NO_2Sty	13 ± 1	19.5	na
3-MeSty	23 ± 1	19.4	na
3-MeOSty	27 ± 1	19.7	na
3-ClSty	20 ± 1	19.9	na
3-FSty	15 ± 1	19.7	na

[a]From ref 33 at 30 °C. na, not available.

Since the addition of peroxyl radical to an alkene is an electrophilic reaction,[34] the polar transition state of the PRA reaction would be opposite to the carbon-radical addition to alkenes, which was a nucleophilic process (Figure 8).[35]

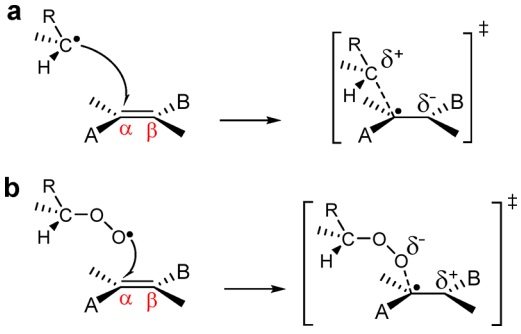

Figure 8. Comparison of the polar transition state between (a) carbon radical and (b) peroxyl radical to an alkene.

Therefore, we hypothesized that the addition rate constant of the peroxyl radical to styrene would increase as the electron density at the double bond increases. We indeed observed an increase in k_{add} values of styrene derivatives with strong electron-donating groups at the para-position such as 4-MeSty and 4-MeOSty. However, the addition rate constants of styrene derivatives with electron-withdrawing groups such as 4-ClSty, 4-FSty, and 4-NO_2Sty were found to have k_{add} values that are similar to that of styrene. This observation suggests that radical stabilization effects are more important than polar effects in influencing the reactivities of PRA to styrene. To provide further insights into our results, we calculated the activation energies for the addition reaction between the peroxyl radical and each of the para-substituted styrenes using the B3LYP/6-31++G(d,p) method (Table 1). In the computational model of the reaction transition state, we used the methyl peroxyl radical as a simplified analogue for the MeLn peroxyl radical to expedite the calculations. Consistent with the measured k_{add} values, we observed a decrease in the computed energy barriers for Sty, 4-MeSty, and 4-MeOSty, respectively. There was also no significant difference in the activation energies of 4-ClSty, 4-FSty, and 4-NO_2Sty from that of Sty, which agreed with our experimental data. The experimental k_{add} values also appear to align better with the trend predicted by the computed spin density than the atomic polar tensor charge, which represents the partial charge distribution (Figure 9a and 9b).

We then attempted to generate a Hammett correlation by plotting $\log(k_X/k_H)$ versus either the σ_{para}-scale[36] or the radical σ-scale (σ_{rad})[37] (Figure S16a and b). However, both Hammett parameters did not allow us to derive a good linear correlation between substituent effects and the rate constant of the PRA reaction. Therefore, we utilized the extended Hammett equation:

$$\log k_X/k_H = \rho\sigma^+ + \sigma_{rad} \quad (6)$$

to derive the correlation between the substituent effects and the computed activation energies (Figure 9e).[38] Note that since the reaction rates appear to be mediated primarily through radical stabilization effects and the transition state contains a partial positive charge, the use of the σ^+-scale[39] is more appropriate than the σ-scale.[36] The values of $\log(k_X/k_H)$, σ^+, and σ_{rad} for each substituent were fit to eq 6, giving a ρ-value of −0.66. Fitting of the calculated activation energy and the combined Hammett parameters ($\sigma_{rad} - 0.66\sigma^+$) with linear regression gave eq 7 (R^2 = 0.85):

$$E_a = -1.04(\sigma_{rad} - 0.66\sigma^+) + 19.4 \text{ (kcal/mol)} \quad (7)$$

which describes the dual radical-cationic properties of the benzylic carbon in styrene and its derivatives (Figure 9c). The negative slope of the line also confirmed that there is a partial positive charge buildup on the benzylic carbon atom during the transition state and that the addition of peroxyl radical to alkene is indeed an electrophilic reaction. Fitting of the calculated activation energy and $\log(k_X/k_H)$ also gave a good linear correlation (R^2 = 0.93) with a negative slope of −1.21, which shows a good agreement between our theoretical and experimental data (Figure 9d). We then examined the meta-substituted styrene derivatives to investigate how the addition rate constants and activation energies would change with only contribution from the polar effects (Table 1). The small changes in both rate constants and activation energies of the meta-substituted styrene derivatives further suggested that the contribution of polar effects to the reactivity of the PRA reaction is small. In addition, the rate constants of the meta-substituted styrene derivatives and σ_{meta} parameters did not give a good linear correlation in the Hammett plot (Figure S16c).

Application of the New Peroxyl Radical Clock Approach to Structure−Reactivity Relationship Studies of Different Oxidizable Substrates. Here, we applied the new peroxyl radical clock approach to measure the values of k_p, k_H, and k_{add} for different series of oxidizable substrates

https://dx.doi.org/10.1021/acs.joc.0c01920
J. Org. Chem. 2021, 86, 153−168

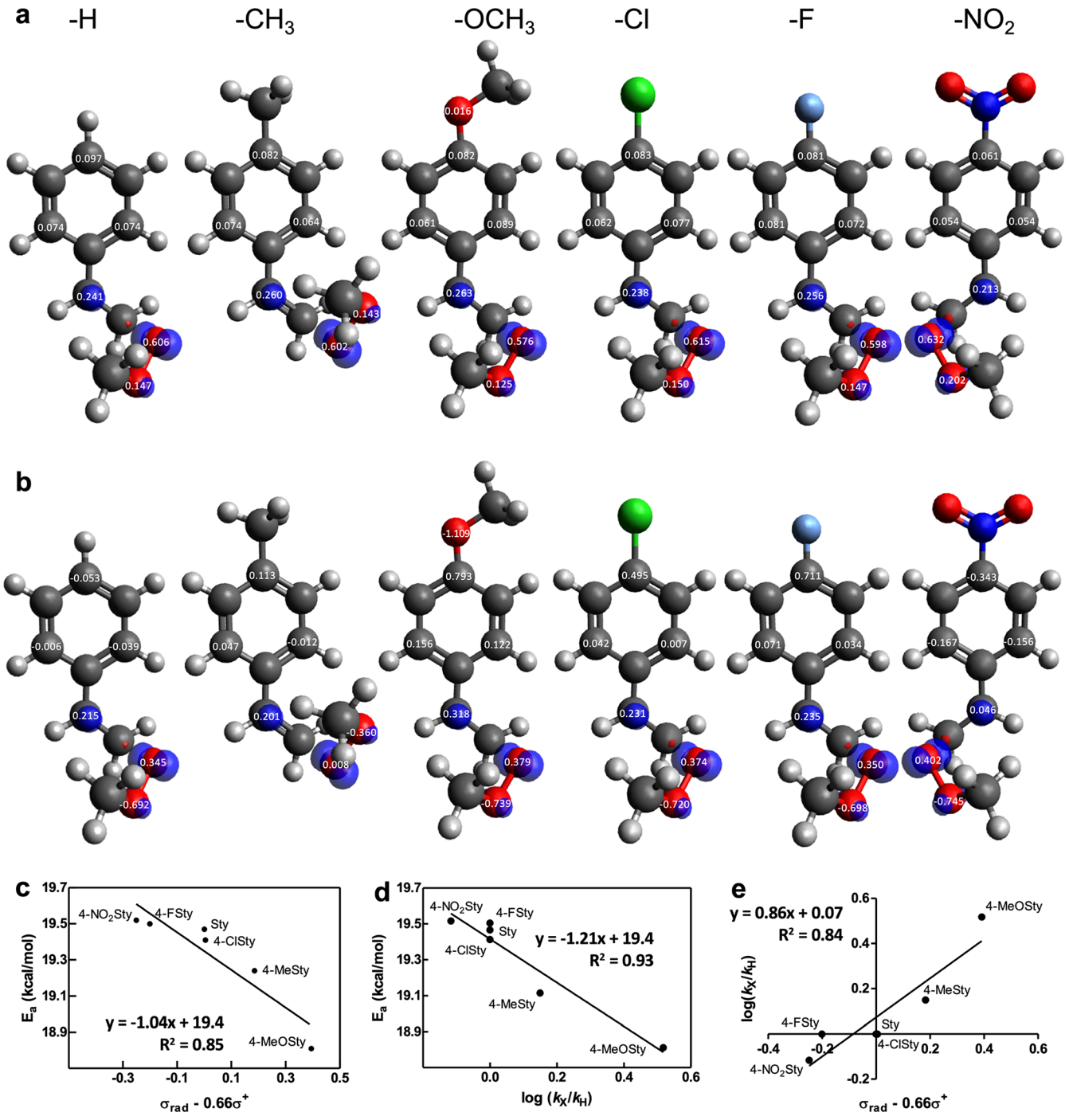

Figure 9. (a) Spin density and (b) atomic polar tensor charge distribution in the transition states; (c) activation energies versus the combination of radical and cation Hammett parameters; (d) activation energies versus $\log(k_X/k_H)$; (e) $\log(k_X/k_H)$ versus the combination of radical and cation Hammett parameters for PRA reactions to the para-substituted styrene derivatives. The atoms displayed are carbon (dark gray), hydrogen (light gray), oxygen (red), chlorine (green), fluorine (light blue), and nitrogen (dark blue).

including α- and β-MeSty, conjugated dienes with different methyl substituents, and cyclic compounds (Figure 4c, d, and e). The results are summarized in Table 2.

Structure−reactivity relationship studies on these substrates allow us to examine the factors that affect the contribution of each mechanism to the overall propagation rate constant. For example, both α- and β-MeSty have significantly different reactivities toward the HAT mechanism due to the location of their methyl substituent. Particularly, while the proposed resulting carbon radicals formed after the abstraction of H atom from α-MeSty span only three carbon centers, the loss of H atom from β-MeSty potentially forms a much more delocalized radical (Figure 10). This explains why β-MeSty has significant contribution from the HAT mechanism while α-MeSty is k_{add} dominant. However, we are surprised by the higher k_{add} value of β-MeSty compared to α-MeSty. The addition of peroxyl radical into the terminal methylene group of α-MeSty would potentially lead to the formation of a tertiary benzylic radical, which is highly stable. While the addition of the peroxyl radical at the same carbon of β-MeSty would

https://dx.doi.org/10.1021/acs.joc.0c01920
J. Org. Chem. 2021, 86, 153−168

Table 2. Free Radical Oxidation Propagation (k_p), Hydrogen-Atom Transfer (k_H), and Peroxyl Radical Addition (k_{add}) Rate Constants of Different Organic Oxidizable Substrates Measured by the New Peroxyl Radical Clock at 37 °C[a]

substrate	k_p (M^{-1} s^{-1})	k_{add}/k_H	k_H (M^{-1} s^{-1})	k_{add} (M^{-1} s^{-1})	lit. k_H (M^{-1} s^{-1})	lit. k_{add} (M^{-1} s^{-1})
α-MeSty	27 ± 1	k_{add} dominant	na	26 ± 2	na	10[a]
β-MeSty	63 ± 1	3.1 ± 0.6	15 ± 2	48 ± 2	na	51[a]
1,3-pentadiene	34 ± 2	k_{add} dominant	na	34 ± 2	na	na
3-methyl-1,3-pentadiene	154 ± 4	k_{add} dominant	na	154 ± 4	na	na
2,4-dimethyl-1,3-pentadiene	97 ± 4	2.4 ± 0.5	29 ± 4	68 ± 4	na	na
1,3-hexadiene	65 ± 1	0.5 ± 0.1	43 ± 3	22 ± 3	na	na
2,4-hexadiene	165 ± 7	1.0 ± 0.3	81 ± 11	84 ± 11	na	na
2,5-dimethyl-2,4-hexadiene	509 ± 73	1.1 ± 0.2	243 ± 21	266 ± 21	na	na
1,3-cyclohexadiene (1,3-CHD)	878 ± 35	0.95 ± 0.12	449 ± 26	429 ± 26	220[b]	na
1,4-cyclohexadiene (1,4-CHD)	478 ± 15	k_H dominant	478 ± 15	na	1480[b] 265[c] 362[d]	na
1,2-dihydronaphthalene	141 ± 8	0.33 ± 0.08	106 ± 6	35 ± 6	52[b]	291[a]
indene	80 ± 5	0.47 ± 0.09	55 ± 3	25 ± 3	14[b]	128[a]
2-methylindene	100 ± 7	1.1 ± 0.3	48 ± 6	52 ± 6	na	na
α-terpinene	1304 ± 11	0.28 ± 0.03	1019 ± 24	285 ± 24	na	na

[a]k_H values are reported as per molecule, instead of per H atom. na, not available. [b]From ref 22 at 30 °C. [c]From ref 23 at 37 °C. [d]From ref 40 at 30 °C.

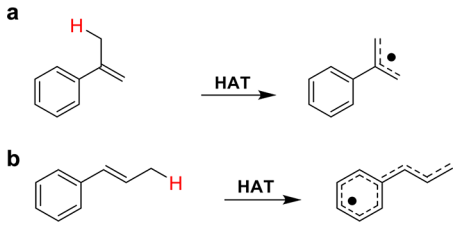

Figure 10. Proposed resulting carbon radicals formed after the HAT reactions from (a) α-MeSty and (b) β-MeSty.

generate a stable secondary benzylic carbon radical, this addition position has a methyl substituent. Thus, one would expect β-MeSty to have lower k_{add} value than α-MeSty. In addition, we want to note the difference in the order of our experimental k_{add} values for Sty, α-MeSty, and β-MeSty from those reported by the rotating-sector method. The discrepancy here can be attributed to the fact that the propagation rate constants depend on the structure of not only the substrate but also the chain-propagating peroxyl radical.[22] Specifically, in the rotating-sector method, the resulting chain-carrying species is a tertial peroxyl radical after the addition of peroxyl radical to α-MeSty, which is a lot more hindered than the secondary peroxyl radicals derived from Sty and β-MeSty.[22] Hence, the rate constant for α-MeSty measured using the rotating-sector method is much smaller than those of Sty and β-MeSty. On the other hand, in the peroxyl radical clock method, the chain-carrying species are the same secondary linoleate-based peroxyl radicals for all substrates, which means the propagation rate constants depend mostly on the structures of the substrates.

Pairwise comparison of substrates from Table 2 also confirms the electronic effects on k_{add}. For example, structures that contain additional methyl substituents on the double bond, including 3-methyl-1,3-pentadiene, 2,4-dimethyl-1,3-pentadiene, 2,4-hexadiene, and 2,5-dimethyl-2,4-hexadiene (Figure 4d), have much higher k_{add} values compared to 1,3-pentadiene. Similarly, the addition of a methyl substituent on 2-methylindene also doubles the k_{add} value of this substrate compared to indene. However, it should be noted that 2,4-dimethyl-1,3-pentadiene has a lower k_{add} value compared to 3-methyl-1,3-pentadiene even though it has more methyl substituents. In 3-methyl-1,3-pentadiene, the peroxyl radical can be added to both carbon 1 and 4. However, in 2,4-dimethyl-1,3-pentadiene, the two methyl substituents at carbon 4 sterically hinder the attack of the peroxyl radical at this position. Comparison between 1,3-pentadiene and 1,3-hexadiene also allowed us to confirm that changes in k_H values are dependent on the stability of the radical formed after the loss of the H atom. Specifically, after the HAT reaction, 1,3-hexadiene would yield a secondary radical that is much more stable than the primary radical formed from 1,3-pentadiene. Hence, 1,3-hexadiene has a much higher k_H value and lower k_{add}/k_H ratio than 1,3-pentadiene.

The difference in reactivities of 1,3-CHD and 1,4-CHD indicates that the PRA mechanism can only significantly contribute to k_p when there is a conjugated double bond system. Specifically, 1,4-CHD has a nonconjugated double bond system with two bis-allylic positions, which have been found to be highly reactive toward H atom transfer.[41] Thus, 1,4-CHD is k_H dominant. In contrast, 1,3-CHD has a conjugated double bond system, which explains why there is significant contribution of k_{add} to its total propagation rate constant. It should be noted that the k_H values measured for 1,3- and 1,4-CHD are almost identical, which is consistent with the similar C−H bond dissociation energies (BDEs) previously reported for the two compounds.[42] We also want to note the discrepancy of our experimental k_H value for 1,4-CHD (478 M^{-1} s^{-1}) compared to the value previously reported (1480 M^{-1} s^{-1}).[22] Similar to the cases of Sty, α-MeSty, and β-MeSty, the difference can probably be attributed to the different propagating radicals between the rotating-sector method and our new peroxyl radical clock approach. Specifically, the chain-carrying species in the oxidation of 1,4-CHD under the rotating-sector method are mainly H−OO· radicals, which is sterically unhindered and highly reactive, thus explaining the larger HAT rate constant.[43] It should be noted that our experimental k_H value for 1,4-CHD is on the same order of magnitude as the previous results in which the chain-carrying species are also linoleate-based peroxyl radicals.[23,40] In addition, Howard and Ingold reported predominant contribu-

https://dx.doi.org/10.1021/acs.joc.0c01920
J. Org. Chem. 2021, 86, 153−168

Table 3. Free Radical Oxidation Propagation (k_p), Hydrogen-Atom Transfer (k_H), and Peroxyl Radical Addition Rate Constants (k_p) of Different Biologically Important Lipids Measured by the New Peroxyl Radical Clock Approach at 37 °C[a]

substrate	k_p (M^{-1} s^{-1})	k_{add}/k_H	k_H (M^{-1} s^{-1})	k_{add} (M^{-1} s^{-1})	lit. k_p (M^{-1} s^{-1})
7-dehydrocholesterol (7-DHC)	2737 ± 83	k_H dominant	2737 ± 83	na	2260[b]
cholesteryl acetate	36 ± 2	k_H dominant	36 ± 2	na	31.4[c]
retinal	5656 ± 143	k_{add} dominant	na	5656 ± 143	na
coenzyme Q10	695 ± 23	k_{add} dominant	na	695 ± 23	na
vitamin D_3	1031 ± 63	1.4 ± 0.4	430 ± 63	601 ± 63	na
conjugated linoleic acid 18:2 (CLA 18:2)	118 ± 8	1.1 ± 1.3	57 ± 21	61 ± 21	na
conjugated linolenic acid 18:3 (CLA 18:3)	1235 ± 60	2.4 ± 1.7	359 ± 117	876 ± 117	na
nonconjugated linolenic acid 18:3 (NLA 18:3)	144 ± 3	k_H dominant	144 ± 3	na	na

[a]k_H values are reported as per molecule, instead of per H atom. na, not available. [b]From ref 24 at 37 °C. [c]From ref 29 at 37 °C.

tion of the PRA mechanism to the propagation rate constants of 1,3-CHD, 1,2-dihydronaphthalene, and indene.[22,42] However, we found that the HAT mechanism contributes more significantly to the propagation step of 1,2-dihydronapthalene and indene, and both mechanisms contribute similarly to the propagation rate constant of 1,3-CHD. This discrepancy may be attributed to the fact that in the rotating-sector method, the H-atom abstracting species are polymeric peroxyl radicals, $R(OOR)_nOO\cdot$, derived from the substrate.[22] Furthermore, the k_{add} values for 1,2-dihydronaphthalene and indene are on the same order of magnitude as those of the styrene derivatives reported here, suggesting consistency when using the radical clock method. Because of the different propagating radicals involved between the rotating-sector method and the peroxyl radical clock method, we suggest that the rate constants measured using the same method would provide better comparison of the reactivity of the oxidizable molecules.

Examination of Reactivities of Biologically Important Lipids. The values of k_p, k_H, and k_{add} for different biologically important lipids including sterols, lipophilic vitamins, and PUFAs were also measured using the new peroxyl radical clock and are reported in Table 3 (Figure 4f).

Due to the low solubility of cholesterol in benzene and hexane, which caused difficulties in both the experimental setup and product analyses, we opted to use its ester analogue, cholesteryl acetate, as the substrate instead. Even though cholesteryl acetate is more reactive toward free radical oxidation than cholesterol, their product distribution was reported to be the same.[29] The k_p values of cholesteryl acetate and 7-DHC measured by the new radical clock are 36 and 2737 M^{-1} s^{-1}, respectively. Both values are close to the previously reported values of 31.4 and 2260 M^{-1} s^{-1}, which were measured using the original peroxyl radical clock method.[24,29] These results validate the applicability of the new approach in examining the rate constants of lipid peroxidation. We found the HAT mechanism to be predominant in cholesteryl acetate, which is consistent with the previous finding that cholesterol addition products only account for 12% of the total oxidation products.[29] Due to the conjugated double bonds in the structure of 7-DHC, we expected to observe significant contribution from the PRA mechanism into the overall rate constant. However, surprisingly, we found 7-DHC to also be k_H dominant. In addition, coenzyme Q10 and lipophilic vitamins such as vitamin D_3 and retinal were all found to be highly reactive toward free radical oxidation with k_p values of 695, 1031, and 5656 M^{-1} s^{-1}, respectively. Significantly, the k_p value of retinal suggested that this compound would replace 7-DHC as the most reactive biological compound toward free radical oxidation known to date. All three compounds were found to have major contribution from the PRA mechanism, which can be attributed to their highly conjugated double bond systems. Likely due to the presence of a tertiary allylic H atom, vitamin D_3 also has significant contribution from HAT.

We then examined the propagation rate constants of different PUFAs, including CLA 18:2, CLA 18:3, and NLA 18:3. As observed in 1,3-CHD and 1,4-CHD, conjugated PUFAs, including CLA 18:2 and CLA 18:3, have significant contribution from the PRA mechanism while nonconjugated PUFAs such as NLA 18:3 are k_H dominant. To our surprise, conjugated PUFAs appeared to be much more reactive toward lipid peroxidation compared to their nonconjugated analogues. For example, the total propagation rate constants for linoleic acid and CLA 18:2 are 62 and 118 M^{-1} s^{-1}, respectively. Similarly, CLA 18:3 was found to be highly reactive with a k_p value of 1235 M^{-1} s^{-1} compared to the k_p value of 144 M^{-1} s^{-1} for NLA 18:3.

DISCUSSION

Factors Controlling the Contribution of the HAT and PRA Reaction to the Overall Propagation Step. In this study, we report the development of a new peroxyl radical clock approach that, for the first time, simultaneously measures the rate constants of the HAT and PRA reactions for a variety of organic and lipid substrates. The structure−reactivity relationship studies through the application of this new approach have allowed us to derive five important factors that influence how each mechanism would contribute to the rate-limiting step of the free radical oxidation mechanism.

(1) Radical stabilization effects are more important than polar effects in influencing the reactivities of the PRA reaction. Through the application of the new peroxyl radical approach to measure the k_{add} values of para- and meta-substituted styrene derivatives, we found that only substituents that allow the delocalization of electron spin via either resonance or hyperconjugation would significantly enhance the reactivities of PRA reactions. This observation is consistent with previously reported results that radical stabilization effects are more important than polar effects in influencing the stability of ring-substituted benzylic radicals.[38,44,45] In addition, we found that the experimental k_{add} values and the computed activation energies of styrene and its para-substituted derivatives agreed better with the computed spin density than the atomic polar tensor charge distribution at the benzylic carbon as seen in Table 1 and Figure 9a and 9b.

Another example for the trend observed here is coenzyme Q10. Specifically, the methoxy moiety, which is an electron-donating substituent, can stabilize the radicals formed after the

https://dx.doi.org/10.1021/acs.joc.0c01920
J. Org. Chem. 2021, 86, 153−168

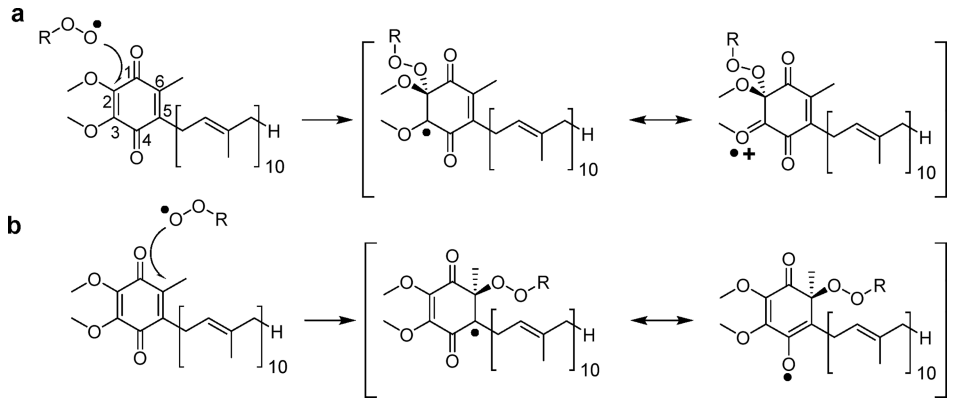

Figure 11. Proposed resonance stabilization of radicals formed after the PRA reaction in coenzyme Q10 by (a) a methoxy group, an electron-donating substituent, and (b) a carbonyl group, an electron-withdrawing substituent.

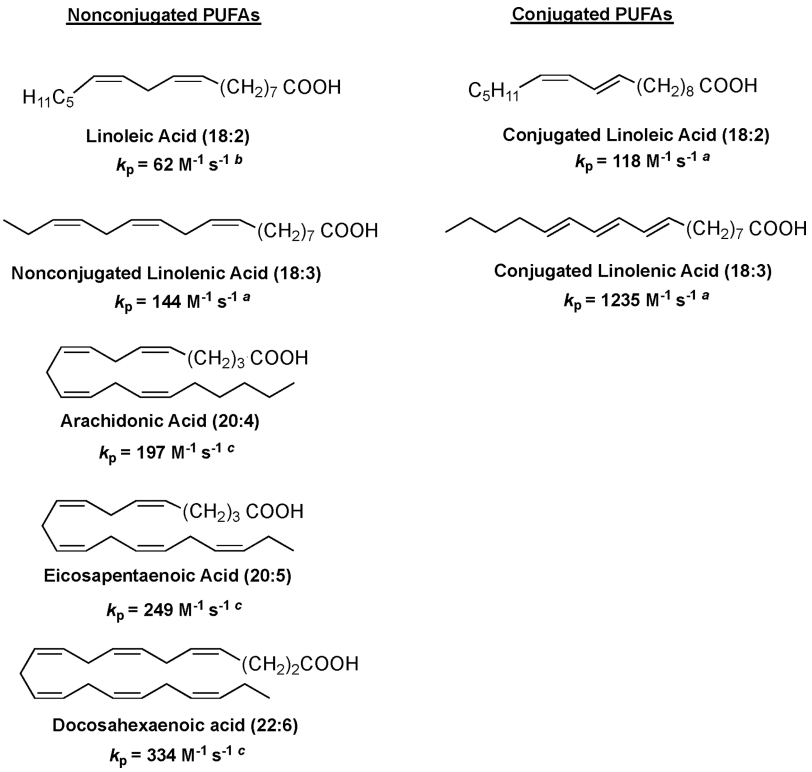

Figure 12. Structures and rate constants of different nonconjugated and conjugated PUFAs. [a]This work. [b]From ref 22. [c]From ref 24.

PRA reaction at C2 or C3 via resonance (Figure 11a). Computational modeling of the transition state of peroxyl radical addition to C2 indicates that the methoxy group, C2, and C3 appear to be in the same plane in the transition state (Figure S15). On the other hand, the radicals formed after the addition of the peroxyl radical into any vinylic carbons can be delocalized into the carbonyl moiety, which is an electron-withdrawing substituent (Figure 11b). Thus, the large k_{add} value of coenzyme Q10 is further evidence that for the PRA mechanism, radical stabilization effects are more important than polar effects.

The small changes in both the measured rate constants and computed activation energies of the meta-substituted styrenes supported our observation that polar effects do not contribute significantly to the PRA mechanism. In the transition state of the addition of peroxyl radical to styrene, there is a development of both radical characteristic and partial positive charge at the benzylic carbon. Therefore, we employed the extended Hammett equation to derive a linear correlation between the computed activation energies and substituents effects via the dual radical-cationic Hammett parameters (Figure 9c). The negative slope of −1.04 confirmed the predicted reaction mechanism.

(2) The PRA mechanism only contributes significantly to the overall propagation rate constant in structures with conjugated double bond systems, and the more conjugated the system is, the larger the increase in the total rate constant. As an example, due to its conjugated double bond system, 1,3-CHD has significant contribution from the PRA mechanism in addition to the HAT reaction and, thus, is much more reactive toward lipid peroxidation compared to its isomer 1,4-CHD, which is k_H dominant. The same trend was also observed in other pairs of isomers investigated in this study, such as NLA and CLA.

https://dx.doi.org/10.1021/acs.joc.0c01920
J. Org. Chem. 2021, 86, 153−168

One of the most surprising and important findings in this study is how much more reactive the conjugated double bond structures are compared to the nonconjugated ones. For example, the total propagation rate constant measured for CLA 18:3 is 10 times that of NLA 18:3, which is due to the combination of both PRA and HAT reactions. In addition, compounds that contain three conjugated double bonds, such as vitamin D_3 and CLA 18:3, were found to have k_p values of over 1000 M^{-1} s^{-1} with significant contribution from both mechanisms. Significantly, retinal has a conjugated system with five double bonds and thus has a propagation rate constant of almost 5700 M^{-1} s^{-1}, which is the largest rate constant that has ever been measured for a lipid molecule.

To fully understand how reactive the conjugated double bond structures are, we compared the increase in the propagation rate constants of different nonconjugated and conjugated PUFAs (Figure 12). Nonconjugated PUFAs such as arachidonic acid, eicosapentaenoic acid, and docosahexaenoic acid are commonly considered highly reactive fatty acids. Their reactivities toward the HAT reaction are attributed to the number of bis-allylic positions due to the weaker C−H bonds at these positions.[41,46,47] Thus, the ratio of the rate constants for linoleic acid, NLA 18:3, arachidonic acid, eicosapentaenoic acid, and docosahexaenoic acid is roughly 1:2:3:4:5, which is proportional to the number of their bis-allylic positions. However, this increase in rate constant is much larger for the conjugated double bond systems. For example, CLA 18:3 has only one more double bond than CLA 18:2, but the difference in their propagation rate constants is 10 times. Based on the result of retinal, we estimated that a structure with five conjugated double bonds would have a k_p value of roughly 6000 M^{-1} s^{-1}, and a structure with four conjugated double bonds would have a rate constant in between 1235 and 6000 M^{-1} s^{-1}.

(3) Monoallylic positions that are adjacent to conjugated double bond system are reactive toward the HAT reaction. Monoallylic H atoms in acyclic structures are commonly believed to be less reactive toward abstraction compared to those at bis-allylic positions. However, once the values of k_{add} and k_H are distinguished for conjugated PUFAs using the new peroxyl radical clock, we found that monoallylic positions that are adjacent to a highly conjugated double bond system are also highly reactive toward HAT reactions. For example, when there is an increase in double bond from CLA 18:2 to 18:3, there is a 6-fold increase in k_H values, though to a lesser extent than the increase in k_{add} values (14-fold). Our results are, in fact, consistent with the findings that C−H BDEs decrease with extended conjugation of lipids.[41] Specifically, the lowest theoretical C−H BDEs calculated for lipids with two and three conjugated double bonds were 77.4 and 72.9 kcal/mol, respectively, comparable to the bis-allylic C−H bond BDE at 72.7 kcal/mol.[41]

(4) Cyclic compounds are more reactive toward lipid peroxidation than their acyclic analogues, but their k_{add}/k_H ratios are the same. The trend that cyclic compounds are more reactive toward lipid peroxidation than their acyclic analogues has previously been discussed.[4] Indeed, we found that 1,3-CHD has a much larger k_p value compared to 1,3-hexadiene and CLA 18:2. However, after measuring the individual k_{add} and k_H, we found that all three compounds have almost the same ratio k_{add}/k_H of one. This indicates that both k_H and k_{add} values are larger in the cyclic compounds than their acyclic analogues.

(5) Steric hindrance and the location of the substituents can potentially affect the reactivity of the PRA mechanism. Despite the opposite polar transition state, factors that affect the reactivities of carbon-radical addition to alkenes can also be applied to PRA to alkenes. The first factor is steric hindrance which can potentially dictate the regioselectivity of both reactions. Specifically, it was found that carbon radicals, and potentially peroxyl radicals, attack alkenes preferentially at the carbon atoms which are the least sterically hindered.[35] The second factor is the location of the substituents. In the addition of carbon radical to alkenes, it was found that a substituent that is bound to the α-carbon, to which the radical is added, exerts markedly different effects compared to a substituent attached to the neighboring carbon (the β-carbon);[35] i.e., the β-substituent only exerts a polar effect on the rate constant while the α-substituent mostly exerts both polar and steric effects, but the polar effect is less than that of the β-substituent. Therefore, we propose that the same principle can be applied to the reaction between peroxyl radical and alkenes. In fact, even though 1,3-hexadiene, 2,4-hexadiene, and 3-methyl-1,3-pentadiene all have an additional methyl group compared to 1,3- pentadiene, only 2,4-hexadiene and 3-methyl-1,3-pentadiene have a substantial increase in k_{add} due to the polar effect of the additional methyl group on the conjugated double bonds. Replacing the methyl with an ethyl group in 1,3-hexadiene and the addition of a methyl on the other end of the alkene in 2,4-hexadiene resulted in substantial k_H, but addition of the methyl at the cross-conjugation position of the alkene in 3-methyl-1,3-pentadiene did not result in an observable k_H. Furthermore, addition of two more terminal methyl groups in 2,5-dimethyl-2,4-hexadiene resulted in large increases in both k_{add} and k_H. On the other hand, the smaller k_{add} value of 2,4-dimethyl-1,3- pentadiene relative to 3-methyl-1,3-pentadiene is likely due to the steric hindrance at one of the terminal vinyl carbons. However, for this series of dienes overall, the steric effect appears to be less important than the radical-stabilizing effect of the additional substituents. Further investigation is required to examine whether a bulkier substituent on the α-carbon could exert a larger steric effect for the PRA reactions.

Limitations of the New Peroxyl Radical Clock Approach. We found that there is a threshold to which the new peroxyl radical clock approach can distinguish between k_H and k_{add} values. Since a PRA-derived epoxide product, 7-DHC 5α,6α-epoxide, was previously detected among the oxidation products of 7-DHC,[12,29,30] we predicted that there should be significant contribution from the PRA mechanism to the peroxidation of 7-DHC. However, our results showed that 7-DHC is k_H dominant. This finding is surprising as we mentioned that structures with conjugated double bonds are expected to have a large k_{add} value. We attempted to resolve this conflict in results by investigating α-terpinene, a compound that shares a cyclic diene and a tertiary monoallylic position with the 7-DHC structure (Figure 4e and Table 2). In fact, the abstraction of an H atom from the tertiary monoallylic position of α-terpinene would yield a highly stable carbon radical. This explains the large increase in both the total propagation and HAT rate constants compared to 1,3-CHD, which only has the cyclic diene in its structure. Significantly, the k_{add}/k_H ratio also decreases from 0.95 in 1,3-CHD to 0.28 in α-terpinene. Compared to α-terpinene, 7-DHC has two tertiary monoallylic positions, a much more rigid structure, and a well-aligned axial C−H bond with the π-orbitals, which requires minimum reorientation of the molecule to reach the

https://dx.doi.org/10.1021/acs.joc.0c01920
J. Org. Chem. 2021, 86, 153−168

transition of HAT.[24,30] Thus, it is reasonable to see that 7-DHC displays a much larger k_H than α-terpinene. On the other hand, a cholestadienol with a similar substitution pattern as α-terpinene has a k_p of 1370 M^{-1} s^{-1}, similar to that of α-terpinene.[48] Although there is contribution from the PRA mechanism to the total propagation rate constant of 7-DHC, the k_{add} value may be too small to be detected by the new radical clock, which relies on accurate determination of the k_{add}/k_H ratio. Similarly, even though 12% of the total oxidation products from cholesterol or cholesteryl acetate were addition products,[29] our new approach was not sensitive enough to measure the k_{add} of this substrate. Therefore, we concluded that there is a threshold of the k_{add}/k_H ratio at which the new radical clock approach can resolve the individual k_{add} and k_H values. In the case where the contribution from one mechanism is significantly less than the other, the new approach is not sensitive enough to resolve them. The lowest k_{add}/k_H ratio that we were able to measure in this study was 0.28 of α-terpinene. Improvement on the new radical clock approach would be needed in the future to overcome this limitation.

Biological Implications of the Lipid Peroxidation Mechanism. The differentiation between HAT and PRA reactions in the propagation step will allow us to better understand not only the lipid peroxidation kinetics and mechanism but also the distribution of the oxidation products of a lipid, which translates into its biological and pathological effects. For example, a lipid that primarily undergoes the PRA mechanism would yield more addition products such as epoxides and, thus, would exert very different biological effects compared to a lipid that predominantly undergoes the HAT mechanism, which generates mostly lipid hydroperoxides. Therefore, it would be interesting to compare the biological effects of nonconjugated PUFAs, which predominantly undergo the HAT reaction, and conjugated PUFAs, which can also undergo PRA in addition to the HAT reaction. Even though the peroxidation reactivities and mechanism of nonconjugated PUFAs, such as arachidonic acid, have been studied extensively,[2,49] to our knowledge, this is the first study that explored the reactivities and mechanism toward lipid peroxidation of conjugated PUFAs, including CLA 18:2 and CLA 18:3. Conjugated linoleic and linolenic acids do not occur naturally in humans and can only be found in meat and dairy products from ruminants and plant-based food products such as pomegranate seed oil and bitter gourd seed.[50−53] However, these conjugated fatty acids have attracted many research efforts due to their health-promoting properties, such as antidiabetic,[54] anti-inflammatory,[55] antiatherogenic,[56] and anticarcinogen.[57,58]

Interestingly, parinaric acid, an 18:4 conjugated fatty acid, is >25 times more cytotoxic to cancer cells than the corresponding nonconjugated fatty acids, and the antioxidant, butylated hydroxytoluene, abolishes its cytotoxicity, indicating a lipid peroxidation-mediated cell death mechanism.[59] Another CLA 18:3, α-eleostearic acid, was recently found to significantly sensitize triple-negative breast cancer cells to ferroptosis,[60] a type of cell death that is tightly associated with lipid peroxidation.[13,14,61] Due to the substantial generation of ROS and constantly being under high levels of oxidative stress,[62] certain types of cancer cell lines rely heavily on the functions of the components in the cellular antioxidant network, including glutathione peroxidase 4 and system x_c^-, for their survival.[13,14] Therefore, inhibition of these two components by RSL3 and erastin, respectively, leads to the accumulation of lipid oxidation products via the free radical chain reactions to lethal levels, resulting in cell death, i.e., ferroptosis.[16] Since lipid peroxidation plays a central role in the execution of ferroptosis, nonconjugated PUFAs, such as arachidonic acid, due to their high reactivities toward lipid peroxidation, have been found to potentiate ferroptosis.[61,63,64] Based on the surprisingly large k_p value measured in this study for conjugated PUFAs, we suggest that the cytotoxicity of conjugated PUFAs to cancer cells can be attributed to its high reactivity toward lipid peroxidation. The ability of conjugated PUFAs to enhance ferroptosis could also be related to their oxidation product distribution, which should be composed of large amounts of addition products, i.e., allylic epoxides. These epoxides are highly electrophilic and can form adducts with macromolecules, such as proteins and DNA, leading to damages.[65,66] Besides conjugated PUFAs, the peroxidation reactivities and mechanism of coenzyme Q10 and lipophilic vitamins, such as retinal and vitamin D_3, were determined for the first time in this study. Coenzyme Q10, retinal, and vitamin D_3 have been found to play important roles in a variety of biological processes.[67−69] However, only the reactivities and peroxidation mechanism of vitamin A precursor, β-carotene, have been studied previously.[70−75] It would be intriguing to explore how the high reactivities of these lipid species would translate into their biological activities, especially in ferroptosis. The exceptionally large rate constant of vitamin A, retinal in this study, is of particular interest because it has been reported to act as both an antioxidant and a pro-oxidant under low and high oxygen tension, respectively.[70−73] Considering the fact that oxygen tension varies significantly in different tissues/organs, vitamin A might play different roles in inducing or inhibiting ferroptosis in different types of cancer cells.

EXPERIMENTAL SECTION

General Methods and Materials. The radical initiator, MeOAMVN, was purchased from Wako Chemicals, dried under vacuum, and stored at −80 °C. MeLn (Nu-Chek-Prep, Inc.) was purified through silica gel (10% ethyl acetate:90% hexane) prior to use and stored at −80 °C. Sty, 4-MeSty, 4-MeOSty, 4-ClSty, 4-FSty, 3-MeSty, 3-MeOSty, 3-ClSty, α-MeSty, (*trans*-)β-MeSty, 1,3-pentadiene, 3-methyl-1,3-pentadiene, 2,4-dimethyl-1,3-pentadiene, 1,3-hexadiene, 2,4-hexadiene, 2,5-dimethyl-2,4-hexadiene, 1,2-dihydronaphthalene, indene, 2-methylindene, and α-terpinene were purchased from Sigma-Aldrich Co. and were purified through a short Al_2O_3 column to remove stabilizers such as 4-*tert*-butylcatechol prior to use. 4-NO_2Sty was purchased from Thermo Fisher Scientific Inc., stored at −20 °C, and purified through a column to remove stabilizers prior to use. 7-DHC was purchased from Sigma-Aldrich Co., stored at −20 °C, and purified through silica gel column prior to use. Cholesteryl acetate was purchased from Thermo Fisher Scientific Inc. and used without further purification. Retinal, coenzyme Q10, and Vitamin D_3 were purchased from Chem-Impex Int'l Inc. and used without further purification. CLA 18:2 and NLA 18:3 were purchased from Nu-Chek-Prep, Inc. and used without further purification. 9(*E*),11(*E*),13(*E*)-CLA 18:3 (≥97%) was purchased from Cayman Chemical and used without further purification. The internal standard, 9-anthracenemethanol (97%), was purchased from Sigma-Aldrich Co. $LiAlH_4$ (1 M in THF) was purchased from Sigma-Aldrich Co. Benzene (HPLC grade) was passed through a column of neutral alumina prior to use. HPLC grade hexanes and isopropyl alcohol were purchased from Thermo Fisher Scientific Inc.

General Procedure for the New Peroxyl Radical Clock Approach Using Methyl Linoleate. The initial experimental setup for the new approach is similar to the conventional peroxyl radical clock method.[23] Briefly, for each reaction, stock solution of the

https://dx.doi.org/10.1021/acs.joc.0c01920
J. Org. Chem. 2021, 86, 153−168

substrate at various amounts was added first to each reaction vial. Then, the same amount of stock solution of MeLn in benzene, an adjusted amount of benzene, and the same amount of stock solution of MeOAMVN in benzene were added to bring the final reaction volume in each vial to 300 μL. The final concentrations of MeLn and MeOAMVN are 0.302 M and 1.5 mM, respectively. Each reaction was carried out at 37 °C for an hour and then quenched by adding butylated hydroxytoluene (50 μL, 0.2 M in benzene) and 9-anthracenemethanol (6 μL, 3 mM in chloroform). The resulting mixture was vortexed for 5 s and left at room temperature for 30 min before splitting into two portions of the same volume. The first portion was diluted with 1 mL of hexane for the analysis of HPODEs by HPLC-UV (Phenomenex Luna 4.6 × 150 mm Si column; 3 μm particle size; 1.0 mL/min; eluting solvent, Hex:Iso = 99.5:0.5). The other half of the reaction mixture was reduced by the addition of $LiAlH_4$ (90 μL, 1 M in THF). The mixture was then vortexed for 5 s, left at room temperature for 15 min, and quenched by the addition of concentrated HCl (20 μL). The final reaction mixture was diluted with 1 mL of hexane, followed by filtration with Teflon syringe filter, for the analysis of HODOLs by HPLC-UV with eluting solvent of Hex:Iso = 95.5:4.5 using the same column. The measurement of rate constants for each substrate is performed in triplicate. The peak areas for HPODEs and HODOLs were integrated at 234 nm. In addition, the peak areas for the internal standard were integrated at 254 nm. The ratio [*t*,*c*-HODOLs]/[*t*,*t*-HODOLs] is calculated as below:

$$\frac{[t,\ c\text{-HODOLs}]}{[t,\ t\text{-HODOLs}]} = \frac{(\text{total areas under all } t,\ c\text{-HODOLs})}{(\text{total areas under all } t,\ t\text{-HODOLs})}$$

The ratio $[\text{HODOL}_{\text{total}}]/[\text{HPODE}_{\text{total}}]$ is calculated as below:

$$\frac{[\text{HODOL}_{\text{total}}]}{[\text{HPODE}_{\text{total}}]} = \frac{(\text{total areas under all HODOLs})/(\text{total area of internal standard})}{(\text{total areas under all HPODEs})/(\text{total area of internal standard})}$$

General Procedure for Free Radical Oxidation of 7-DHC with the New Peroxyl Radical Clock Approach. The oxidation, reduction, and HPLC-UV analysis for 7-DHC were carried out similarly as described above. However, the stock solution of 7-DHC was prepared in a solvent mixture of an equal amount of chlorobenzene and benzene (chlorobenzene:benzene = 1:1). The reaction was also carried out in chlorobenzene:benzene to increase the solubility of 7-DHC.

General Procedure for Free Radical Oxidation of Retinal with the New Peroxyl Radical Clock Approach. The oxidation, reduction, and HPLC-UV analysis for retinal were carried out similarly as described above, but the experiment was carried out in only 30 min instead of 1 h.

General Procedure for Free Radical Oxidation of NLA 18:2, CLA 18:2, and CLA 18:3 with the New Peroxyl Radical Clock Approach. The oxidation, reduction, and HPLC-UV analysis for NLA 18:2, CLA 18:2, and CLA 18:3 were carried out similarly as described above. However, the −OOH moiety in these three fatty acids gives a broad peak in the HPLC chromatograms that overlaps with the HPODEs product peaks. Therefore, to avoid this overlapping, the nonreduced reaction mixture of these three compounds was analyzed using an eluting solvent of Hex:Iso = 99.864:0.136.

Preparation of HODOLs. A large-scale autoxidation was carried out using 5 g of methyl linoleate and 5 mol % of MeOAMVN at 37 °C. The product mixture was then quenched by the addition of BHT and then reduced with $LiAlH_4$ at 0 °C. After an excess amount of $LiAlH_4$ was quenched with concentrated HCl, the solution was neutralized by the addition of saturated $NaHCO_3$ solution until there were no bubbles. The resulting solution was then extracted with methylene chloride and ethyl acetate and concentrated. The product mixture was then first purified by flash column chromatography to enrich HODOL-containing fractions and remove the majority of reduced methyl linoleate. Part of the HODOL mixture was then subject to purification by HPLC (250 × 10 mm Si column; 5 μm; 6 mL/min; eluting solvent, Hex:Iso = 95.5:4.5) to obtain individual HODOLs. Ag^+-coordination electrospray ionization analysis of individual HODOLs on a high-resolution QTOF mass spectrometer (Waters Synapt XS) revealed expected doublets due to the isotopes of Ag (^{107}Ag and ^{109}Ag) (Figure S14).

13-trans, trans-HODOL. ^{1}H NMR ($CDCl_3$, 300 MHz): 0.88 (t, 3H, *J* = 6.8 Hz), 1.30 and 1.56 (br s, 20H), 2.07 (q, 2H, *J* = 6.9 Hz), 3.64 (t, 2H, *J* = 6.6 Hz), 4.11 (q, 1H, *J* = 6.5 Hz), 5.57 (dd, 1H, *J* = 7.0 and 15.1 Hz), 5.70 (dt, 1H, *J* = 7.2 and 14.9 Hz), 6.02 (dd, 1H, *J* = 10.4 and 15.0 Hz), 6.17 (dd, 1H, *J* = 10.4 and 15.2 Hz). ^{13}C NMR ($CDCl_3$, 500 MHz): 14.06, 22.62, 25.15, 25.72, 29.09, 29.19, 29.36, 29.41, 31.81, 32.63, 32.81, 37.33, 63.10, 72.93, 129.50, 130.96, 133.69, 135.51. HRMS $[M + {}^{107}Ag]^+$ ($C_{18}H_{34}AgO_2$): observed, 389.1652; theoretical, 389.1604. UV−vis: λ_{max} (in hexanes) = 230.9 nm.

9-trans, trans-HODOL. ^{1}H NMR ($CDCl_3$): ^{1}H NMR ($CDCl_3$, 300 MHz): 0.89 (t, 3H, *J* = 6.8 Hz), 1.31 and 1.56 (br s, 20H), 2.07 (q, 2H, *J* = 6.9 Hz), 3.64 (t, 2H, *J* = 6.6 Hz), 4.10 (q, 1H, *J* = 6.5 Hz), 5.57 (dd, 1H, *J* = 7.0 and 15.0 Hz), 5.70 (dt, 1H, *J* = 7.2 and 14.9 Hz), 6.02 (dd, 1H, *J* = 10.4 and 14.9 Hz), 6.17 (dd, 1H, *J* = 10.4 and 14.9 Hz). ^{13}C NMR ($CDCl_3$, 500 MHz): 14.06, 22.54, 25.43, 25.72, 28.93, 29.36, 29.50, 29.52, 31.43, 32.63, 32.81, 37.33, 63.10, 72.91, 129.42, 131.01, 133.61, 135.66. HRMS $[M + {}^{107}Ag]^+$ ($C_{18}H_{34}AgO_2$): observed, 389.1652; theoretical, 389.1604. UV−vis: λ_{max} (in hexanes) = 230.9 nm.

13-trans, cis-HODOL. HRMS $[M + {}^{107}Ag]^+$ ($C_{18}H_{34}AgO_2$): observed, 389.1639; theoretical, 389.1604. UV−vis: λ_{max} (in hexanes) = 234.4 nm.

9-trans, cis-HODOL. HRMS $[M + {}^{107}Ag]^+$ ($C_{18}H_{34}AgO_2$): observed, 389.1644; theoretical, 389.1604. UV−vis: λ_{max} (in hexanes) = 234.4 nm.

Computational Method. All geometry optimization was performed using the Gaussian 16 software[76] with the hybrid density functional B3LYP and the 6-31++G(d,p) basis. Transition state optimization and calculations, including activation energies, spin densities, and atomic polar tensor charge distribution, were also carried out using the B3LYP/6-31++G(d,p) with QST2 method. The activation energies were calculated by deducting the sum of total energies (electronic + thermal free energies) of styrene derivatives and methyl peroxyl radicals from the total energies (electronic + thermal free energies) of the transition state.

■ ASSOCIATED CONTENT

Supporting Information

The Supporting Information is available free of charge at https://pubs.acs.org/doi/10.1021/acs.joc.0c01920.

Experimental data (XLSX)

Supplementary data of k_{add} and k_H calculations of all substrates; HPLC chromatograms of representative substrates; characterization of HODOL products, including HPLC/UV, mass spectrometry, and NMR data; computational modeling of the addition of methyl peroxyl radical to coenzyme Q_{10}; supplementary data of the generation of Hammett plots; activation energies and Cartesian coordinates for styrene and its derivatives (PDF)

■ AUTHOR INFORMATION

Corresponding Author

Libin Xu − *Department of Medicinal Chemistry, University of Washington, Seattle, Washington 98195, United States;* orcid.org/0000-0003-1021-5200; Phone: (206) 543-1080; Email: libinxu@uw.edu; Fax: (206) 685-3252

Authors

Quynh Do − *Department of Medicinal Chemistry, University of Washington, Seattle, Washington 98195, United States*

https://dx.doi.org/10.1021/acs.joc.0c01920
J. Org. Chem. 2021, 86, 153−168

David D. Lee − *Department of Medicinal Chemistry, University of Washington, Seattle, Washington 98195, United States*
Andrew N. Dinh − *Department of Medicinal Chemistry, University of Washington, Seattle, Washington 98195, United States*; orcid.org/0000-0002-9708-4583
Ryan P. Seguin − *Department of Medicinal Chemistry, University of Washington, Seattle, Washington 98195, United States*
Rutan Zhang − *Department of Medicinal Chemistry, University of Washington, Seattle, Washington 98195, United States*

Complete contact information is available at: https://pubs.acs.org/10.1021/acs.joc.0c01920

Notes

The authors declare no competing financial interest.

■ ACKNOWLEDGMENTS

This work is supported by a grant from the National Science Foundation (CHE-1664851). The authors thank Dylan H. Ross for helping with setting up the transition state calculations using Gaussian.

■ REFERENCES

(1) Ray, P. D.; Huang, B. W.; Tsuji, Y. Reactive oxygen species (ROS) homeostasis and redox regulation in cellular signaling. *Cell. Signalling* **2012**, *24* (5), 981−90.
(2) Yin, H.; Xu, L.; Porter, N. A. Free Radical Lipid Peroxidation: Mechanisms and Analysis. *Chem. Rev.* **2011**, *111* (10), 5944−5972.
(3) Halliwell, B.; Chirico, S. Lipid peroxidation: Its mechanism, measurement, and significance. *Am. J. Clin. Nutr.* **1993**, *57* (5), 715S−725S.
(4) Xu, L.; Porter, N. A. Free radical oxidation of cholesterol and its precursors: Implications in cholesterol biosynthesis disorders. *Free Radical Res.* **2015**, *49* (7), 835−849.
(5) Brown, A. J.; Jessup, W. Oxysterols and atherosclerosis. *Atherosclerosis* **1999**, *142* (1), 1−28.
(6) Davi, G.; Falco, A.; Patrono, C. Lipid peroxidation in diabetes mellitus. *Antioxid. Redox Signaling* **2005**, *7* (1−2), 256−68.
(7) Ames, B. N. DNA damage from micronutrient deficiencies is likely to be a major cause of cancer. *Mutat. Res., Fundam. Mol. Mech. Mutagen.* **2001**, *475* (1−2), 7−20.
(8) Barrera, G. Oxidative stress and lipid peroxidation products in cancer progression and therapy. *ISRN Oncol* **2012**, *2012*, 137289.
(9) Simonian, N. A.; Coyle, J. T. Oxidative stress in neurodegenerative diseases. *Annu. Rev. Pharmacol. Toxicol.* **1996**, *36*, 83−106.
(10) Sayre, L. M.; Zelasko, D. A.; Harris, P. L.; Perry, G.; Salomon, R. G.; Smith, M. A. 4-Hydroxynonenal-derived advanced lipid peroxidation end products are increased in Alzheimer's disease. *J. Neurochem.* **1997**, *68* (5), 2092−7.
(11) Porter, F. D.; Scherrer, D. E.; Lanier, M. H.; Langmade, S. J.; Molugu, V.; Gale, S. E.; Olzeski, D.; Sidhu, R.; Dietzen, D. J.; Fu, R.; Wassif, C. A.; Yanjanin, N. M.; Marso, S. P.; House, J.; Vite, C.; Schaffer, J. E.; Ory, D. S. Cholesterol oxidation products are sensitive and specific blood-based biomarkers for Niemann-Pick C1 disease. *Sci. Transl. Med.* **2010**, *2* (56), 56ra81.
(12) Xu, L.; Korade, Z.; Rosado, D. A.; Liu, W.; Lamberson, C. R.; Porter, N. A. An oxysterol biomarker for 7-dehydrocholesterol oxidation in cell/mouse models for Smith-Lemli-Opitz syndrome. *J. Lipid Res.* **2011**, *52* (6), 1222−1233.
(13) Dixon, S. J.; Lemberg, K. M.; Lamprecht, M. R.; Skouta, R.; Zaitsev, E. M.; Gleason, C. E.; Patel, D. N.; Bauer, A. J.; Cantley, A. M.; Yang, W. S.; Morrison, B., 3rd; Stockwell, B. R. Ferroptosis: an iron-dependent form of nonapoptotic cell death. *Cell* **2012**, *149* (5), 1060−72.
(14) Yang, W. S.; SriRamaratnam, R.; Welsch, M. E.; Shimada, K.; Skouta, R.; Viswanathan, V. S.; Cheah, J. H.; Clemons, P. A.; Shamji, A. F.; Clish, C. B.; Brown, L. M.; Girotti, A. W.; Cornish, V. W.; Schreiber, S. L.; Stockwell, B. R. Regulation of ferroptotic cancer cell death by GPX4. *Cell* **2014**, *156* (1−2), 317−331.
(15) Zilka, O.; Shah, R.; Li, B.; Friedmann Angeli, J. P.; Griesser, M.; Conrad, M.; Pratt, D. A. On the Mechanism of Cytoprotection by Ferrostatin-1 and Liproxstatin-1 and the Role of Lipid Peroxidation in Ferroptotic Cell Death. *ACS Cent. Sci.* **2017**, *3* (3), 232−243.
(16) Shah, R.; Shchepinov, M. S.; Pratt, D. A. Resolving the Role of Lipoxygenases in the Initiation and Execution of Ferroptosis. *ACS Cent. Sci.* **2018**, *4* (3), 387−396.
(17) Conrad, M.; Pratt, D. A. The chemical basis of ferroptosis. *Nat. Chem. Biol.* **2019**, *15* (12), 1137−1147.
(18) Porter, N. A. A Perspective on Free Radical Autoxidation: The Physical Organic Chemistry of Polyunsaturated Fatty Acid and Sterol Peroxidation. *J. Org. Chem.* **2013**, *78* (8), 3511−3524.
(19) Zielinski, Z. A. M.; Pratt, D. A. Lipid Peroxidation: Kinetics, Mechanisms, and Products. *J. Org. Chem.* **2017**, *82* (6), 2817−2825.
(20) Howard, J.; Ingold, K. Absolute Rate Constants for Hydrocarbon Autoxidation: IV. Tetralin, Cyclohexene, Diphenylmethane, Ethylbenzene, And Allylbenzene. *Can. J. Chem.* **1966**, *44*, 1119−1130.
(21) Howard, J. A.; Ingold, K. U.; Symonds, M. Absolute rate constants for hydrocarbon oxidation. VIII. The reactions of cumylperoxy radicals. *Can. J. Chem.* **1968**, *46* (6), 1017−1022.
(22) Howard, J.; Ingold, K. Absolute rate constants for hydrocarbon autoxidation. VI. Alkyl aromatic and olefinic hydrocarbons. *Can. J. Chem.* **1967**, *45*, 793−802.
(23) Roschek, B.; Tallman, K. A.; Rector, C. L.; Gillmore, J. G.; Pratt, D. A.; Punta, C.; Porter, N. A. Peroxyl Radical Clocks. *J. Org. Chem.* **2006**, *71* (9), 3527−3532.
(24) Xu, L.; Davis, T. A.; Porter, N. A. Rate Constants for Peroxidation of Polyunsaturated Fatty Acids and Sterols in Solution and in Liposomes. *J. Am. Chem. Soc.* **2009**, *131* (36), 13037−13044.
(25) Lamberson, C. R.; Muchalski, H.; McDuffee, K. B.; Tallman, K. A.; Xu, L.; Porter, N. A. Propagation rate constants for the peroxidation of sterols on the biosynthetic pathway to cholesterol. *Chem. Phys. Lipids* **2017**, *207*, 51−58.
(26) Pratt, D. A.; Tallman, K. A.; Porter, N. A. Free Radical Oxidation of Polyunsaturated Lipids: New Mechanistic Insights and the Development of Peroxyl Radical Clocks. *Acc. Chem. Res.* **2011**, *44* (6), 458−467.
(27) Kresge, N.; Simoni, R. D.; Hill, R. L. The Biosynthetic Pathway for Cholesterol: Konrad Bloch. *J. Biol. Chem.* **2005**, *280* (10), e7.
(28) Holick, M. F.; Frommer, J. E.; McNeill, S. C.; Richtand, N. M.; Henley, J. W.; Potts, J. T., Jr. Photometabolism of 7-dehydrocholesterol to previtamin D3 in skin. *Biochem. Biophys. Res. Commun.* **1977**, *76* (1), 107−14.
(29) Zielinski, Z. A. M.; Pratt, D. A. H-Atom Abstraction vs Addition: Accounting for the Diverse Product Distribution in the Autoxidation of Cholesterol and Its Esters. *J. Am. Chem. Soc.* **2019**, *141* (7), 3037−3051.
(30) Xu, L.; Korade, Z.; Porter, N. A. Oxysterols from Free Radical Chain Oxidation of 7-Dehydrocholesterol: Product and Mechanistic Studies. *J. Am. Chem. Soc.* **2010**, *132* (7), 2222−2232.
(31) Liu, W.; Porter, N. A.; Schneider, C.; Brash, A. R.; Yin, H. Formation of 4-hydroxynonenal from cardiolipin oxidation: Intramolecular peroxyl radical addition and decomposition. *Free Radical Biol. Med.* **2011**, *50* (1), 166−178.
(32) Baschieri, A.; Pizzol, R.; Guo, Y.; Amorati, R.; Valgimigli, L. Calibration of Squalene, p-Cymene, and Sunflower Oil as Standard Oxidizable Substrates for Quantitative Antioxidant Testing. *J. Agric. Food Chem.* **2019**, *67* (24), 6902−6910.
(33) Howard, J. A.; Ingold, K. U. Absolute Rate Constants for Hydrocarbon AutoxidatioN: I. Styrene. *Can. J. Chem.* **1965**, *43* (10), 2729−2736.

(34) Stark, M. S. Addition of Peroxyl Radicals to Alkenes and the Reaction of Oxygen with Alkyl Radicals. *J. Am. Chem. Soc.* **2000**, *122* (17), 4162−4170.
(35) Giese, B. Formation of CC Bonds by Addition of Free Radicals to Alkenes. *Angew. Chem., Int. Ed. Engl.* **1983**, *22* (10), 753−764.
(36) McDaniel, D. H.; Brown, H. C. An Extended Table of Hammett Substitutent Constants Based on the Ionization of Substituted Benzoic Acids. *J. Org. Chem.* **1958**, *23* (3), 420−427.
(37) Fisher, T. H.; Meierhoefer, A. W. Substituent effects in free-radical reactions. A study of 4-substituted 3-cyanobenzyl free radicals. *J. Org. Chem.* **1978**, *43* (2), 224−228.
(38) Dinçtürk, S.; Jackson, R. A.; Townson, M. An improved $\sigma\cdot$ scale. The thermal decomposition of substituted dibenzylmercury compounds in alkane solutions. *J. Chem. Soc., Chem. Commun.* **1979**, *4*, 172−174.
(39) Taylor, R. *Electrophilic aromatic substitution*; John Wiley: Chichester, England; New York, 1990; *pp xvi*, 513.
(40) Porter, N. A.; Lehman, L. S.; Weber, B. A.; Smith, K. J. Unified mechanism for polyunsaturated fatty acid autoxidation. Competition of peroxy radical hydrogen atom abstraction, .beta.-scission, and cyclization. *J. Am. Chem. Soc.* **1981**, *103* (21), 6447−6455.
(41) Pratt, D. A.; Mills, J. H.; Porter, N. A. Theoretical Calculations of Carbon−Oxygen Bond Dissociation Enthalpies of Peroxyl Radicals Formed in the Autoxidation of Lipids. *J. Am. Chem. Soc.* **2003**, *125* (19), 5801−5810.
(42) Korcek, S.; Chenier, J.; Howard, J.; Ingold, K. Absolute Rate Constants for Hydrocarbon Autoxidation. XXI. Activation Energies for Propagation and the Correlation of Propagation Rate Constants with Carbon−Hydrogen Bond Strengths. *Can. J. Chem.* **1972**, *50*, 2285−2297.
(43) Howard, J. A.; Ingold, K. U. Absolute rate constants for hydrocarbon autoxidation. V. The hydroperoxy radical in chain propagation and termination. *Can. J. Chem.* **1967**, *45* (8), 785−792.
(44) Pratt, D. A.; DiLabio, G. A.; Mulder, P.; Ingold, K. U. Bond Strengths of Toluenes, Anilines, and Phenols: To Hammett or Not. *Acc. Chem. Res.* **2004**, *37* (5), 334−340.
(45) Bathelt, C. M.; Ridder, L.; Mulholland, A. J.; Harvey, J. N. Aromatic Hydroxylation by Cytochrome P450: Model Calculations of Mechanism and Substituent Effects. *J. Am. Chem. Soc.* **2003**, *125* (49), 15004−15005.
(46) Trenwith, A. B. Dissociation of 3-methylpenta-1, 4-diene and the resonance energy of the pentadienyl radical. *J. Chem. Soc., Faraday Trans. 1* **1982**, *78* (10), 3131−3136.
(47) Berkowitz, J.; Ellison, G. B.; Gutman, D. Three methods to measure RH bond energies. *J. Phys. Chem.* **1994**, *98* (11), 2744−2765.
(48) Xu, L.; Porter, N. A. Reactivities and Products of Free Radical Oxidation of Cholestadienols. *J. Am. Chem. Soc.* **2014**, *136* (14), 5443−5450.
(49) Aliwarga, T.; Raccor, B. S.; Lemaitre, R. N.; Sotoodehnia, N.; Gharib, S. A.; Xu, L.; Totah, R. A. Enzymatic and free radical formation of cis- and trans- epoxyeicosatrienoic acids in vitro and in vivo. *Free Radical Biol. Med.* **2017**, *112*, 131−140.
(50) Dhiman, T. R.; Anand, G. R.; Satter, L. D.; Pariza, M. W. Conjugated linoleic acid content of milk from cows fed different diets. *J. Dairy Sci.* **1999**, *82* (10), 2146−56.
(51) Destaillats, F.; Trottier, J. P.; Galvez, J. M.; Angers, P. Analysis of alpha-linolenic acid biohydrogenation intermediates in milk fat with emphasis on conjugated linolenic acids. *J. Dairy Sci.* **2005**, *88* (9), 3231−9.
(52) Suzuki, R.; Noguchi, R.; Ota, T.; Abe, M.; Miyashita, K.; Kawada, T. Cytotoxic effect of conjugated trienoic fatty acids on mouse tumor and human monocytic leukemia cells. *Lipids* **2001**, *36* (5), 477−82.
(53) Kohno, H.; Suzuki, R.; Noguchi, R.; Hosokawa, M.; Miyashita, K.; Tanaka, T. Dietary conjugated linolenic acid inhibits azoxymethane-induced colonic aberrant crypt foci in rats. *Jpn. J. Cancer Res.* **2002**, *93* (2), 133−42.
(54) Moloney, F.; Toomey, S.; Noone, E.; Nugent, A.; Allan, B.; Loscher, C. E.; Roche, H. M. Antidiabetic effects of cis-9, trans-11-conjugated linoleic acid may be mediated via anti-inflammatory effects in white adipose tissue. *Diabetes* **2007**, *56* (3), 574−82.
(55) Dipasquale, D.; Basirico, L.; Morera, P.; Primi, R.; Troscher, A.; Bernabucci, U. Anti-inflammatory effects of conjugated linoleic acid isomers and essential fatty acids in bovine mammary epithelial cells. *Animal* **2018**, *12* (10), 2108−2114.
(56) Nicolosi, R. J.; Rogers, E. J.; Kritchevsky, D.; Scimeca, J. A.; Huth, P. J. Dietary conjugated linoleic acid reduces plasma lipoproteins and early aortic atherosclerosis in hypercholesterolemic hamsters. *Artery* **1997**, *22* (5), 266−77.
(57) Scimeca, J. A.; Thompson, H. J.; Ip, C. Effect of Conjugated Linoleic Acid on Carcinogenesis. In *Diet and Breast Cancer*; Weisburger, E. K., Ed.; Springer US: Boston, MA, 1994; pp 59−65.
(58) Igarashi, M.; Miyazawa, T. Newly recognized cytotoxic effect of conjugated trienoic fatty acids on cultured human tumor cells. *Cancer Lett.* **2000**, *148* (2), 173−9.
(59) Cornelius, A. S.; Yerram, N. R.; Kratz, D. A.; Spector, A. A. Cytotoxic effect of cis-parinaric acid in cultured malignant cells. *Cancer Res.* **1991**, *51* (22), 6025−6030.
(60) Beatty, A.; Singh, T.; Tyurina, Y. Y.; Nicolas, E.; Maslar, K.; Zhou, Y.; Cai, K. Q.; Tan, Y.; Doll, S.; Conrad, M.; Bayır, H.; Kagan, V. E.; Rennefahrt, U.; Peterson, J. R. Conjugated linolenic fatty acids trigger ferroptosis in triple-negative breast cancer. *bioRxiv* **2019**, 556084.
(61) Yang, W. S.; Kim, K. J.; Gaschler, M. M.; Patel, M.; Shchepinov, M. S.; Stockwell, B. R. Peroxidation of polyunsaturated fatty acids by lipoxygenases drives ferroptosis. *Proc. Natl. Acad. Sci. U. S. A.* **2016**, *113* (34), E4966−75.
(62) Szatrowski, T. P.; Nathan, C. F. Production of Large Amounts of Hydrogen Peroxide by Human Tumor Cells. *Cancer Res.* **1991**, *51* (3), 794.
(63) Doll, S.; Proneth, B.; Tyurina, Y. Y.; Panzilius, E.; Kobayashi, S.; Ingold, I.; Irmler, M.; Beckers, J.; Aichler, M.; Walch, A.; Prokisch, H.; Trümbach, D.; Mao, G.; Qu, F.; Bayir, H.; Füllekrug, J.; Scheel, C. H.; Wurst, W.; Schick, J. A.; Kagan, V. E.; Angeli, J. P. F.; Conrad, M. ACSL4 dictates ferroptosis sensitivity by shaping cellular lipid composition. *Nat. Chem. Biol.* **2017**, *13* (1), 91−98.
(64) Dixon, S. J.; Winter, G. E.; Musavi, L. S.; Lee, E. D.; Snijder, B.; Rebsamen, M.; Superti-Furga, G.; Stockwell, B. R. Human Haploid Cell Genetics Reveals Roles for Lipid Metabolism Genes in Nonapoptotic Cell Death. *ACS Chem. Biol.* **2015**, *10* (7), 1604−1609.
(65) Zhang, J.; Wang, C.; Ji, L.; Liu, W. Modeling of Toxicity-Relevant Electrophilic Reactivity for Guanine with Epoxides: Estimating the Hard and Soft Acids and Bases (HSAB) Parameter as a Predictor. *Chem. Res. Toxicol.* **2016**, *29* (5), 841−850.
(66) Koskinen, M.; Plná, K. Specific DNA adducts induced by some mono-substitued epoxides in vitro and in vivo. *Chem.-Biol. Interact.* **2000**, *129* (3), 209−229.
(67) Zile, M. H. Function of vitamin A in vertebrate embryonic development. *J. Nutr.* **2001**, *131* (3), 705−8.
(68) Holick, M. F. Vitamin D: importance in the prevention of cancers, type 1 diabetes, heart disease, and osteoporosis. *Am. J. Clin. Nutr.* **2004**, *79* (3), 362−71.
(69) Lenaz, G.; Fato, R.; Formiggini, G.; Genova, M. L. The role of Coenzyme Q in mitochondrial electron transport. *Mitochondrion* **2007**, *7* (Suppl), S8−33.
(70) Burton, G. W.; Ingold, K. U. beta-Carotene: an unusual type of lipid antioxidant. *Science* **1984**, *224* (4649), 569−73.
(71) Kennedy, T. A.; Liebler, D. C. Peroxyl radical scavenging by beta-carotene in lipid bilayers. Effect of oxygen partial pressure. *J. Biol. Chem.* **1992**, *267* (7), 4658−63.
(72) Palozza, P.; Calviello, G.; Bartoli, G. M. Prooxidant activity of beta-carotene under 100% oxygen pressure in rat liver microsomes. *Free Radical Biol. Med.* **1995**, *19* (6), 887−92.
(73) Tsuchihashi, H.; Kigoshi, M.; Iwatsuki, M.; Niki, E. Action of beta-carotene as an antioxidant against lipid peroxidation. *Arch. Biochem. Biophys.* **1995**, *323* (1), 137−47.

https://dx.doi.org/10.1021/acs.joc.0c01920
J. Org. Chem. 2021, 86, 153−168

(74) Mordi, R. C.; Walton, J. C.; Burton, G. W.; Hughes, L.; Ingold, K. U.; Lindsay, D. A. Exploratory study of β-carotene autoxidation. *Tetrahedron Lett.* **1991**, *32* (33), 4203−4206.
(75) Mordi, R. C.; Walton, J. C.; Burton, G. W.; Hughes, L.; Keith, I. U.; David, L. A.; Douglas, M. J. Oxidative degradation of β-carotene and β-apo-8′-carotenal. *Tetrahedron* **1993**, *49* (4), 911−928.
(76) Frisch, M. J.; Trucks, G. W.; Schlegel, H. B.; Scuseria, G. E.; Robb, M. A.; Cheeseman, J. R.; Scalmani, G.; Barone, V.; Petersson, G. A.; Nakatsuji, H.; Li, X.; Caricato, M.; Marenich, A. V.; Bloino, J.; Janesko, B. G.; Gomperts, R.; Mennucci, B.; Hratchian, H. P.; Ortiz, J. V.; Izmaylov, A. F.; Sonnenberg, J. L.; Williams; Ding, F.; Lipparini, F.; Egidi, F.; Goings, J.; Peng, B.; Petrone, A.; Henderson, T.; Ranasinghe, D.; Zakrzewski, V. G.; Gao, J.; Rega, N.; Zheng, G.; Liang, W.; Hada, M.; Ehara, M.; Toyota, K.; Fukuda, R.; Hasegawa, J.; Ishida, M.; Nakajima, T.; Honda, Y.; Kitao, O.; Nakai, H.; Vreven, T.; Throssell, K.; Montgomery, J. A., Jr.; Peralta, J. E.; Ogliaro, F.; Bearpark, M. J.; Heyd, J. J.; Brothers, E. N.; Kudin, K. N.; Staroverov, V. N.; Keith, T. A.; Kobayashi, R.; Normand, J.; Raghavachari, K.; Rendell, A. P.; Burant, J. C.; Iyengar, S. S.; Tomasi, J.; Cossi, M.; Millam, J. M.; Klene, M.; Adamo, C.; Cammi, R.; Ochterski, J. W.; Martin, R. L.; Morokuma, K.; Farkas, O.; Foresman, J. B.; Fox, D. J. *Gaussian 16*, Rev. C.01; Gaussian, Inc.: Wallingford, CT, 2016.

https://dx.doi.org/10.1021/acs.joc.0c01920
J. Org. Chem. 2021, 86, 153−168